



UNIVERSITÀ  
DEGLI STUDI  
FIRENZE

# FLORE

## Repository istituzionale dell'Università degli Studi di Firenze

### **A novel kinematic architecture for portable hand exoskeletons**

Questa è la versione Preprint (Submitted version) della seguente pubblicazione:

*Original Citation:*

A novel kinematic architecture for portable hand exoskeletons / Conti, Roberto; Meli, Enrico; Ridolfi, Alessandro. - In: MECHATRONICS. - ISSN 0957-4158. - STAMPA. - 35:(2016), pp. 192-207. [10.1016/j.mechatronics.2016.03.002]

*Availability:*

The webpage <https://hdl.handle.net/2158/1041751> of the repository was last updated on 2021-03-29T17:42:48Z

*Published version:*

DOI: 10.1016/j.mechatronics.2016.03.002

*Terms of use:*

Open Access

La pubblicazione è resa disponibile sotto le norme e i termini della licenza di deposito, secondo quanto stabilito dalla Policy per l'accesso aperto dell'Università degli Studi di Firenze (<https://www.sba.unifi.it/upload/policy-oa-2016-1.pdf>)

*Publisher copyright claim:*

Conformità alle politiche dell'editore / Compliance to publisher's policies

Questa versione della pubblicazione è conforme a quanto richiesto dalle politiche dell'editore in materia di copyright.

This version of the publication conforms to the publisher's copyright policies.

La data sopra indicata si riferisce all'ultimo aggiornamento della scheda del Repository FloRe - The above-mentioned date refers to the last update of the record in the Institutional Repository FloRe

(Article begins on next page)

# A novel kinematic architecture for portable hand exoskeletons

R. Conti\*, E. Meli\*, A. Ridolfi\*

*\* University of Florence  
Department of Industrial Engineering (DIEF)  
Via di Santa Marta 3, 50139, Florence, Italy  
Tel.: +39-055-2758764  
Fax: +39-055-2758755  
corresponding author: roberto.conti@unifi.it*

---

## Abstract

Basing on strict requirements of portability, **low cost** and modularity, an assistive device for **hand-opening impairment**, characterized by an innovative mechanism, has been developed and tested by the authors. This robotic orthosis is designed to be a low-cost and portable hand exoskeleton to assist people with **hand-opening impairment** in their everyday lives. The mechanism has been especially studied for this kind of applications and presents some interesting features in terms of limited encumbrances and costs. Concerning the **hand-opening impairment**, the authors have also developed a methodology which, starting from the geometrical characteristics of the patient's hand, properly defines the novel kinematic mechanism that better fits the finger trajectories. The authors have tested and validated the proposed approach by building a **functional Hand Exoskeleton System (HES)** prototype. The preliminary testing phase of the prototype with a **single subject** is concluded; currently, **a group of subjects is testing the proposed HES methodology in collaboration with a rehabilitation center.**

**Keywords:** Portable Robotics, Hand Exoskeleton, Wearable Robotics, Hand impairments, Exoskeletons, Biorobotics

---

## 1. Introduction

Nowadays, the main cause of adult disability in Europe is the cerebral vascular stroke in which at least 80% of stroke survivors suffer hemiparesis of the upper arm [1], [2]. In particular, both post-stroke survivors and genetic disease patients can suffer hand function impairments in the opening gesture [1]. The study of hand opening assistive robotic devices [3], [4], [5] has rapidly increased to better support different patients' needs and requirements, since hand gestures play a crucial role in daily living activities (e.g. grasping objects, writing, driving, **shaking** hands, etc.).

In the literature, two approaches are mainly presented: the use of artificial muscle stimulation and the support of wearable assistive robotic devices (Figure 1-(a)). Functional Electrical Stimulation (FES) allows the stimulation of muscles that are no longer receiving signals from the central nervous system [6]. The main drawbacks related to this approach are the high invasiveness of the devices, the limited usability and the fast fatigue affecting the patients, and the reduced applicability to patients with limited muscular recruitment abilities. More effective solutions may be provided by robotic devices such as Hand Exoskeleton Systems (HESs), especially designed to assist and to improve the mobility of the patients' hands. Particularly, **HESs** can lead both to the recovery of different manipulation tasks (such as dexterous manipulation and

power grasping) and to the development of rehabilitative devices (to speed up the disease recovery).

The authors fully endorse the robotic approach (Figure 1-(b)), aiming at the development and design of an innovative hand exoskeleton system focused on portability, modularity and **affordability requirements**: the objective is to obtain a light and wearable solution based on the needs of a **specific subject** (called Testing Hand 1,  $TH_1$ ). **The  $TH_1$  subject** is affected by a particular hand opening impairment caused by a genetic disease, Spinal Muscular Atrophy. Therefore, the HES will have to be able to support his daily life activities for several hours during a day.

The development of portable robotic devices is really challenging, because it requires additional limitations in terms of encumbrances, weight and autonomy. However, at the same time, thanks to effectiveness of such solutions, the improvement of the manipulation and **grasping abilities of the subject** may bring him to a substantial recovery of the social interaction gestures in his everyday life (e.g. **shaking** hands, grasping and release of small objects, etc.).

According to the state of the art [3], [4], as regards the linking system between the hand and the exoskeleton, there are two different approaches: single-phalanx devices, in which the robot exchanges forces at the fingertip [7],[8], and multi-phalanx ones, where the device

directly controls each phalanx of the hand [9], [10], [11]. The latter approach leads to more complex mechanisms and control strategies; on the contrary, single-phalanx approach is more suitable for the application of higher forces and for the use of simple actuation systems and control algorithms but it is characterized by intrinsic engineering problems such as the limited space for the physical interaction between the hand and the mechanism. Many examples of multi-phalanx devices can be found in haptics (where the portability requirement is not a constraint) and they are usually used to simulate the virtual-environment interactions [12].

Concerning the mechanism, several rigid **multi-degree-of-freedom** (DOF) kinematic chains have been proposed [13], [14], [15], [16], [17], [18] with few examples of single DOF mechanisms [19]. Nevertheless, the current solutions of single-DOF mechanisms are mainly related to the assistance of the grasping gestures but with very simplified kinematics [19]. In recent years, the spread of soft-robotic applications has led to some preliminary examples of HES based on elastomeric materials or fluid structures [20], [21].

As regards the actuation systems, cable-driven solutions are widely employed for their implicit simplicity [22], [23], [24], while rigid actuator architectures (based on linear actuators or hydraulic ones) may have problems due to the weights and encumbrances [25], [26].

By focusing on the HESs based on single-phalanx solution, rigid mechanism and cable-driven architecture, there are few examples found in literature and most of them use actuation systems separated by the device (usually the device is installed on the hand and the motors are placed on the ground) [3], [27], [28]. Only a narrow part of these examples use motors directly placed on the hand back (extraordinary portability but limited in terms of device performance, due to the weight, and high cost). [29] describes a HES based on a 3DOFs mechanism with 3 electric motors which is very powered (flexo-extension with 5 N maximum force) and precise but very heavy and bulky (0.5 kg and maximum height with respect to the hand back of 8 cm for the one finger mechanism). An interesting solution is described in [30], where the authors developed a 4 DOFs mechanism (1 actuated and 3 passive) for the finger which is able to apply a continuous force of 45 N within a total weight of 1 kg. The drawback of this solution is the high vertical encumbrance and the impossibility to apply this mechanism to all the four fingers. To reduce the encumbrance and the weight, in [31] a device is proposed based on linear electric actuators on a mechanism with 2 DOFs for each finger which allows a maximum force of 10 N, a reduced vertical encumbrance (maximum 6 cm with respect to the hand back) and a weight of 0.5 kg for the whole device.

By following this approach, inspired by the extreme portability and affordability, the authors have developed a new finger mechanism with 1DOF to obtain a full actuation of each finger (1 DOF mechanism for 1 electric rotative actu-

ator) built through a 3D printing machine in a thermoplastic polymer, Acrylonitrile Butadiene Styrene (ABS). Thus, the total weight of the device is about 0.35 kg with a vertical encumbrance of 4 cm. In addition, the authors have put their attention on the cost of the device; in literature, any research article exploits the total cost of its prototype. Our device has been developed and not too limited for a total cost of about 500 €. To summarize, in this re-



Figure 1: Examples of a FES system [6] (a) and of a Hand Exoskeleton System [12] (b)

search work, both the use of a dedicated Motion Capture (MoCap) system and the implementation of a complete 3D multibody model of the HES (model-based approach) have been exploited to design a new single phalanx, rigid, single DOF and cable-driven mechanism for hand exoskeletons aimed at **subjects affected by hand-opening impairment** (see the attached video). During the modelling phase, to develop the HES for a subject ( $TH_1$ ) (who is unable to voluntarily open his hands), the phalanx trajectory acquisitions on a **normal hand subject** ( $TH_2$ , able to voluntarily open and close his hands) have been initially carried out. After that, through the inverse kinematic model of the  $TH_2$  hand, the typical articulation joint variables related to those gestures are obtained. **In this manner, it is possible to simulate the opening and closing gesture for the  $TH_1$  subject (because the  $TH_1$  subject is unable to autonomously open his hands).** The articulation joint variables are then applied to the  $TH_1$  hand multibody model (scaled using the proper geometrical characteristics of  $TH_1$ ) to obtain the same hand gestures and, through the MoCap system, are experimentally validated. Finally, using articulation joint variables, numerical simulations of the  $TH_1$  patient hand have been performed, both for a simulated opening and closing gesture, called virtual opening and closing gesture. Fingertip trajectories obtained through the previous simulations are then used both for an estimation of the natural phalanx trajectories and for the synthesis of a suitable mechanism able to properly reproduce such curves (see Par. 4.2).

The achievement of a trade-off between accuracy and functionality in achieving this crucial task has been reached through a suitable kinematic chain (based on a 1 DOF mechanism) especially developed to reproduce the desired fingertip trajectories. The proposed 1 DOF mechanism is new in the exoskeleton field and turned out to be

quite promising.

The results obtained from the modelling phase have been used in the design phase to develop two versions of the real HES prototype (Fig. 2), **for both the subjects**.

The HES architecture consists of a mechanical part, designed to be modular, stiff and wearable, and an electronic one (actuation system and control unit). The mechanical parts were internally produced by means of the 3D printing machine of the MDM Lab (DIEF, Italy) in order to evaluate, through a **functional prototype**, the performance of the mechanism.

In this paper, after the description of the mechanism synthesis, some preliminary results obtained using **the functional prototype** will be presented. The preliminary testing phase of the prototype with **a single subject** has been concluded; currently, through the collaboration with an Italian rehabilitation center, **a group of subjects** are testing the proposed HES methodology.

## 2. General Architecture of the System

In this chapter, both the methodology to design the HES and the general architecture of the proposed system are described. The proposed HES can be defined as a single phalanx, single DOF, rigid and cable driven system for the fingers without the thumb module (since **the  $TH_1$  subject** maintains a high residual capacity for the thumb). HES's characteristics were chosen according to strict requirements of portability, **affordability and modularity** (Fig. 2).

The connection point between hand and exoskeleton is placed on the intermediate phalanx, but for sake of ergonomics, in the HES prototype also the distal phalanx is connected to the mechanism through a thimble (without changing the mechanism kinematics). Through this approach, the MetaCarpophalangeal (MCP) self alignment problem [32], [33] is overcome by only considering the fingertip trajectories. As briefly said in the introduction, the innovative kinematic chain developed in this research work was designed through the use of a MoCap system (based on a Full-HD camera with slow motion rate and a 2D acquisition software) and preliminarily simulated through a complete multibody model of the hand exoskeleton system.

In the first part of the research activity: starting from the phalanx trajectories of the  $TH_2$  acquired through the MoCap system, a multibody model of the  $TH_2$  hand able to properly simulate the real hand behaviour has been implemented and then validated through the comparison with the real trajectories. This phase has been uniquely carried out for **the  $TH_2$  subject** who is able to voluntarily open and close his hands. Using inverse kinematics, the typical articulation joint variables for these gestures (**opening and closing**) have been calculated. Finally, through the same articulation joint variables, a virtual campaign of acquisition for **the  $TH_1$  subject** has been carried out by means of the related hand multibody model



Figure 2: The developed HES prototype tested by **the  $TH_1$  subject**

(**both for a virtual opening and closing gestures**).

In the second part of the research activity, different kinematics for the exoskeleton mechanisms (both with 1 and 2 DOFs) have been tested for the  $TH_1$  patient; after an analysis in terms of encumbrances and stiffness, the proposed 1 DOF kinematics (single phalanx, rigid and cable-driven architecture based on the new parallel kinematic chain) has been selected. The selection of this solution was mainly related to the capacity of well reproducing the phalanx trajectories (calculated in the previous phase) and to its easier actuation. To validate the HES model by means of the real prototype, **a proposed test case for the experimental validation** to compare the trajectories of the mechanism key points acquired through the MoCap system to the simulated ones has been performed **both for the opening and for the closing phases**.

The final phase of the research activity consists of three different steps: the design phase of the real HES to obtain a portable and modular mechanism, the MoCap validation of the whole HES multibody model (including **both the HES and the hand models**) and the evaluation of the HES transparency (the capability of the HES prototype in reproducing the real trajectories of the hand phalanges). The design of the real HES takes into account the results obtained from the hand exoskeleton multibody model. The proposed methodology (model-based approach) has led the authors to determine the most suitable mechanism which fits the finger trajectories. The design of actuation and control system is based on strict portability **and affordability** requirements; a MicroMaestro device characterized by very reduced encumbrances is used. The placement of the actuators is also a critical aspect for the

usability of the device: to improve the portability and the modularity of the device, the authors proposed to place the actuators directly on the hand (Fig. 2). The main advantages are the reliability and the effectiveness of the direct connection between fingers and actuators but both the inertia and the encumbrances of the HES increase. The choice of the actuators will be related to the required sizes, weights and forces. The control unit and the batteries are integrated into a small box placed on the forearm where **the subject** is able to control the HES only employing two open-close buttons.

### 3. Hand model

Because of the portability and the modularity requirements, the development of a novel kinematic chain in the field of hand exoskeletons is mandatory; therefore, before the design phase of the exoskeleton, a complete kinematic and dynamic analysis of the hand is carried out. For this reason, this section is organized into the following logical steps:

- **Data acquisition:** it consists of the complete geometrical data of the **two different subjects' hands** ( $TH_1$  and  $TH_2$ , see Fig. 3 and Tables 1-2) having different characteristics in terms of size and functionality. A Motion Capture (MoCap) system is then used to obtain the real phalanx trajectories for **the  $TH_2$  subject** needed to validate the model (Fig. 4) and to extract the proper articulation joint variables employed to obtain the same trajectories for **the  $TH_1$  subject** (both **for opening and closing gestures**).
- **Kinematic model:** a simplified model of the hand is used to reproduce the real phalanx trajectories. In particular, by using a planar 3 Revolute manipulator (e.g. RRR manipulator, see Fig. 5) for each finger and its inverse kinematics, it was possible to extract the articulation joint variables of **the  $TH_2$  subject** (both for a closing and an opening gestures) to be used also for **the  $TH_1$  subject**.
- **Dynamic model:** a complete 3D hand model has been developed to simulate the dynamic behaviour of the real hands (see Fig. 6). The dynamic model has been implemented both for the  $TH_1$  and the  $TH_2$  patients. In particular, the  $TH_1$  dynamic model uses the articulation joint variables extracted from the  $TH_2$  **opening and closing gestures**. Therefore, by using the dynamic model, a **proposed test case for the experimental validation** of the  $TH_1$  opening and closing gestures can be performed as well. As regards the dynamic model, it consists of a 3D hand multibody model, an actuation model and a joint limit model, to obtain a realistic behaviour of the hands. In particular, the actuation model applies finger torques to replicate the desired articulation joint variables, while the joint limit model is able to simulate the effects

due to the real articulation limits. In fact, it applies a reaction torque when the bodies reach their position limits (upper and lower limits), depending on the angular position of the phalanges.

- **Simulation results and experimental data:** a **proposed test case for the experimental validation** has been carried out both for the  $TH_1$  and the  $TH_2$  **subjects** to validate the hand models and the model-based methodology. In Fig. 7, a comparison between the simulated finger trajectories and the real ones for the  $TH_2$  is shown (for the index finger). The articulation joint variables obtained from the  $TH_2$  model are then employed to reproduce the virtual opening and closing also for **the  $TH_1$  subject** (Fig. 8).

All the aforementioned models have been implemented **in the Matlab environment**, thanks both to Simulink and Simmechanics tools [34]. The hand model acquisition and validation through the MoCap system are shown in the 1st step of the video.

#### 3.1. Hand model: data acquisition

The data acquisition part is mainly based on the assessment of **the  $TH_2$  subject** phalanx trajectories for each finger, acquired during both the hand **opening and closing gestures** through a MoCap software (Kinovea, open source [35]), as visible in Fig. 4. The marked phalanges are **the proximal, the intermediate and the distal phalanges**. The MoCap system consists of a MoCap software and a Full-HD camera with slow motion rate (see Fig. 4). In addition, **both for the patients  $TH_1$  and  $TH_2$** , the real geometric and dynamic characteristics have been briefly reported in the anthropometric tables Tab.1-2. The geometrical characteristics are basically the phalanx lengths  $l_j^i$  and the radii  $r_j^i$ . These physical parameters were directly measured on the **subjects' hands**.

Table 1:  $TH_1$  Subject characteristics [cm]

	1st phalanx $[l_1^i, r_1^i]$	2nd phalanx $[l_2^i, r_2^i]$	3rd phalanx $[l_3^i, r_3^i]$
Little finger	[3.3, 0.6]	[2.3, 0.6]	[2, 0.6]
Ring finger	[4.8, 0.8]	[3, 0.7]	[2.1, 0.7]
Middle finger	[5.3, 0.8]	[2.9, 0.75]	[2.4, 0.7]
Index finger	[4.5, 0.8]	[2.6, 0.75]	[2.2, 0.7]
Thumb finger	[4.8, 1]	[3.6, 0.9]	[2.8, 0.8]

In Fig. 3, both the hands are shown; in particular, **the  $TH_1$  subject's pathology** causes a deformation of the hand back due to the absence of the muscles needed to perform the hand opening. Therefore this effect has to be taken into account both in the multibody model and in the design phase (to improve the ergonomics of the prototype).

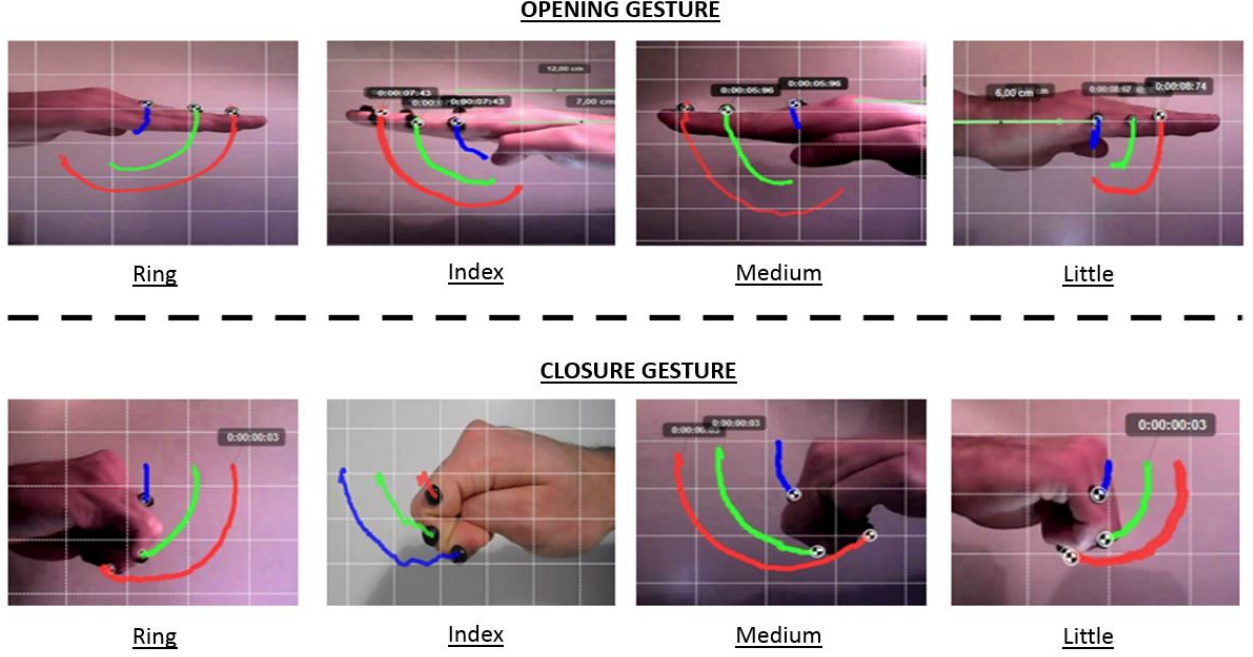


Figure 4: MoCap acquisitions of the  $TH_2$  subject's hand, both for the opening and closing gestures

Table 2:  $TH_2$  Subject characteristics [cm]

	1st phalanx $[l_1^i, r_1^i]$	2nd phalanx $[l_2^i, r_2^i]$	3rd phalanx $[l_3^i, r_3^i]$
Little finger	[3.4, 0.65]	[2, 0.6]	[2, 0.55]
Ring finger	[4, 0.75]	[3, 0.7]	[2.5, 0.7]
Middle finger	[4.5, 0.85]	[3.3, 0.8]	[2.6, 0.8]
Index finger	[4, 0.85]	[2.5, 0.75]	[2, 0.7]
Thumb finger	[4.8, 1]	[3.5, 0.95]	[2, 0.85]

### 3.2. Hand model: kinematic model

To achieve the aim of the research, the proposed hand model is developed by reducing the global DOFs of the system and its complexity: the thumb movements are neglected (because the patient disability does not affect the thumb), rigid bodies are considered to model the hand parts such as the forearm, the palm and the phalanges (proximal, intermediate and distal ones), the links among the phalanges are described by simple rotational joints having fixed revolute axes and the abduction and adduction movements of the MetaCarpophalangeal (MCP) joints are neglected (the rotations are only performed with respect to the local z-axis, see Fig. 5). Finally, of this step of the research, the wrist is fixed.

Assuming the aforementioned hypotheses, the kinematic model of each finger of the hand can be considered as a planar 3R mechanism (Fig. 5) which defines the fingertip pose  $\underline{P}^i(\underline{\Theta}^i)$  as a function of the joint coordinates

#### $TH_1$ patient



#### $TH_2$ patient



Figure 3: Real subject hands:  $TH_1$  and  $TH_2$  comparison

$$\underline{\Theta}^i = [\Theta_1^i \ \Theta_2^i \ \Theta_3^i]^T:$$

$$\underline{P}^i(\underline{\Theta}^i) = [p_x^i \ p_y^i \ \phi^i]^T = \begin{bmatrix} l_1^i c_1 + l_2^i c_{12} + l_3^i c_{123} \\ l_1^i s_1 + l_2^i s_{12} + l_3^i s_{123} \\ \Theta_1^i + \Theta_2^i + \Theta_3^i \end{bmatrix}; \quad (1)$$

where, for example  $c_{12} = \cos(\Theta_1 + \Theta_2)$  and  $s_{12} = \sin(\Theta_1 + \Theta_2)$ ,  $\underline{P}^i$  is the fingertip pose, the apex  $i$  defines the finger ( $i = 1, 2, 3, 4$  starting from the index and excluding the thumb) and  $l_1^i, l_2^i, l_3^i$  are the phalanx lengths.

In Fig. 5, through the reference systems  $\{O_0, x_0, y_0, z_0\}$ ,  $\{O_1^i, x_1^i, y_1^i, z_1^i\}$ ,  $\{O_2^i, x_2^i, y_2^i, z_2^i\}$ ,  $\{O_3^i, x_3^i, y_3^i, z_3^i\}$ , the phalanx lengths  $l_1^i, l_2^i, l_3^i$  and the distance vector between the wrist and the MetaCarpophalangeal joint  $l_0^i$ , the 3R mechanism can be easily adapted to different hand characteristics.

As regards the inverse kinematics of the 3R model, by

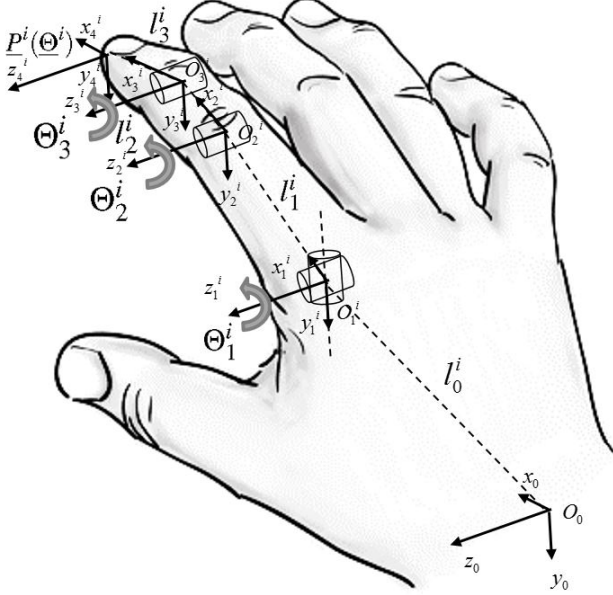


Figure 5: Hand kinematic model

means of Eq. 2 it is possible to obtain the proper articulation angular variables  $\Theta_{des}^i$  starting from the desired fingertip poses  $\underline{P}_{des}^i = [P_{xdes}^i \ P_{ydes}^i \ \Phi_{zdes}^i]^T$ :

$$\begin{cases} \Theta_{1des}^i = a \tan 2(s_1, c_1) \\ \Theta_{2des}^i = a \tan 2(s_2, c_2) \\ \Theta_{3des}^i = \phi^i - \Theta_{1des}^i + \Theta_{2des}^i \end{cases} ; \quad (2)$$

where, this time  $c_1 = \frac{(l_1 + l_2 c_2) P_{xdes}^i - l_2 s_2 P_{ydes}^i}{P_{xdes}^i{}^2 + P_{ydes}^i{}^2}$ ,  $s_1 = \pm \sqrt{1 - c_1^2}$ ,  $c_2 = \frac{P_{xdes}^i{}^2 + P_{ydes}^i{}^2 - l_1^2 - l_2^2}{2l_1 l_2}$  and  $s_2 = \pm \sqrt{1 - c_2^2}$ . The outputs of the inverse kinematic model for each finger are the desired joint trajectories  $\Theta_{des}^i$ . This way, the articulation joint variable for the  $TH_2$  can be extracted starting from the acquired fingertip trajectories. The same angular joint variables are then applied to the hand model of  $TH_1$  to obtain the virtual fingertip trajectories of virtual closing and opening gestures.

### 3.3. Hand model: dynamic model

The hand dynamic model has been developed to assess the kinematic and dynamic interactions between the hand and the exoskeleton. The model consists of different parts:

the multibody model of the hand, the joint limit model and the joint actuator system. The simulation campaign with the dynamic model is performed by defining two simulation modes: hand flexion and hand extension. The hand flexion is **controlled by the subject** and is called ‘**hand closing**’, while the hand extension has to be controlled by the exoskeleton and is called ‘**hand opening**’. In Fig. 6, the 3D dynamic model of the hand is represented and some different subsystems are defined:

- **Multibody model:** it represents the kinematic and dynamic model of the hand where all the geometrical and mass/inertia characteristics are defined for each phalanx (obtained by the 3D analysis). The inputs are both the torques applied by the joint actuators (internal interactions) and the generalized forces applied by the exoskeleton (external interactions); the output is the global hand motion.
- **Joint limit models:** this subsystem is able to simulate the effects due to the real articulation limits. The joint limit models apply a reaction torque depending on the angular position of the phalanges when the bodies reach the limits (upper and lower limits). The inputs are the angular coordinates of the joints and the outputs are the reaction torques calculated through a non-linear function of the angular quantities.
- **Joint actuators:** the actuation of the phalanges is carried out through torques, depending on the simulation mode (‘**hand closing**’-‘**hand opening**’) and on **the subject**. In fact, during the hand opening, major resistance torques have been observed in **the  $TH_1$  subject**, as compared to the  $TH_2$ . More particularly, two different types of torques are applied on the joints: the resistance torques applied during the hand opening phase and the closing torques applied during the **hand closing** one. In the hand opening mode, the exoskeleton opens the fingers (active exoskeleton - passive hand). Therefore, to better simulate the real  $TH_1$  **subject**’s behaviour, when the hand is opened by an external device, variable resistance torques, depending on the phalanx configurations, are applied. As visible in Fig. 6, in this case the inputs are the joint angular coordinates and the outputs are the joint torques. On the contrary, during the hand closing mode, the torques are voluntarily applied by the patient to close the hand (active hand - passive exoskeleton); therefore, PID controllers are used to produce the torques needed to follow the desired trajectory while closing the hand. The inputs are both the desired joint motion  $\Theta_{des}^i$  and the simulated joint angular coordinates  $\Theta_{sim}^i$ ; the outputs are the joint torques.

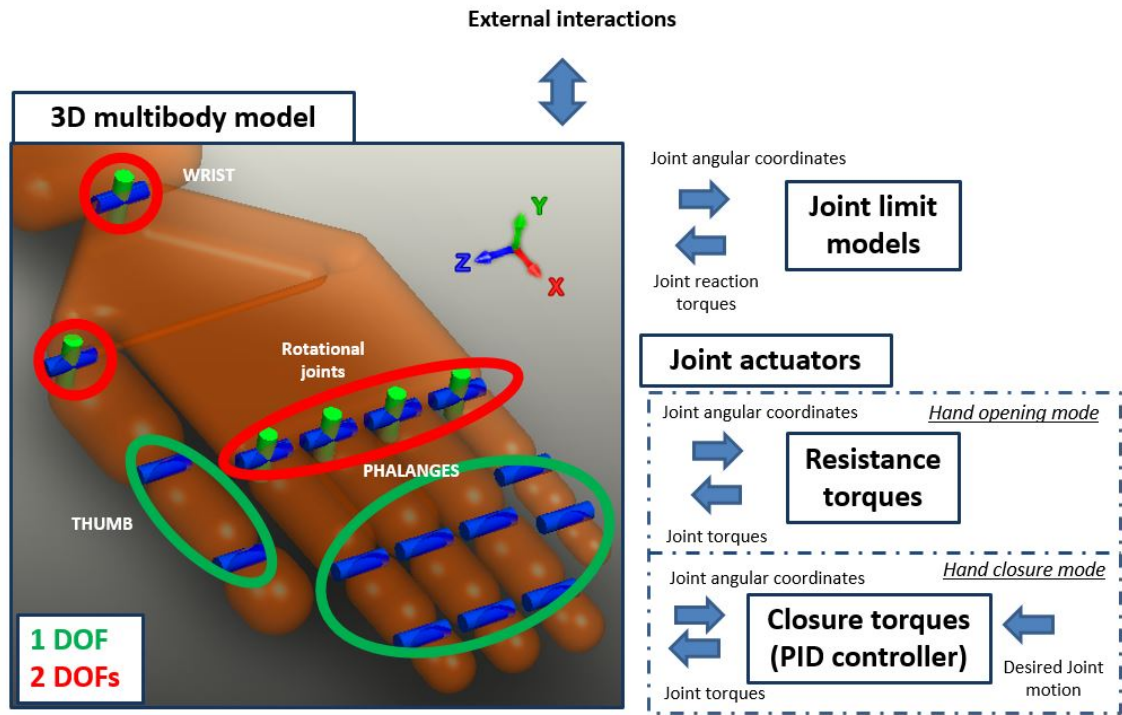


Figure 6: Architecture of the hand dynamic model

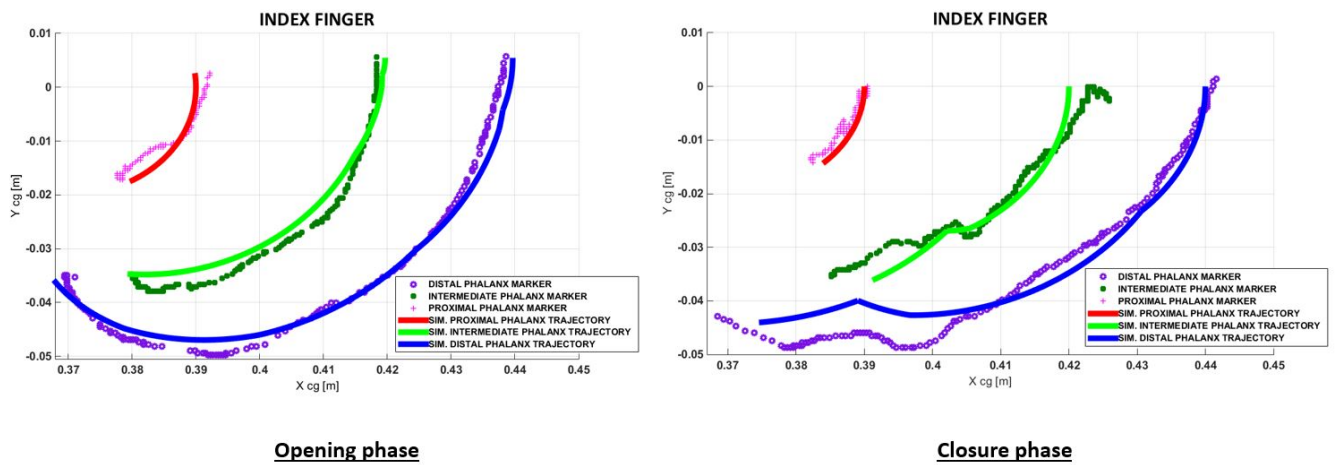


Figure 7:  $TH_2$  subject: comparison between the hand model trajectories and the real ones for the index, respectively during the opening and the closing gestures

### 3.4. Hand model: simulation results and experimental data

In this part, the hand model simulation results will be shown and analysed both for the  $TH_1$  and for the  $TH_2$  subjects. In fact, the first step consists in the validation of the  $TH_2$  hand dynamic model by comparing the real phalanx trajectories acquired by the MoCap software (visible in Fig. 4) with the simulated ones. The  $TH_2$  model is validated for all the fingers both in the opening and in the **closing gestures**. In Fig. 7, for sake of brevity, only the comparison for the index finger is reported; the comparison between the simulated and the acquired trajectories highlights a satisfactory agreement in terms of phalanx trajectories: the proximal phalanx trajectories are the red curves, the intermediate phalanx ones are the green curves and the distal phalanx ones are blue (the values of abscissa  $X_{CG}$  are taken with respect to the geometrical center of the forearm). **The simulated trajectories of the phalanges properly track the real acquisitions; this way, the mean error along the whole trajectories is less than 3 mm while the maximum error is less than 7 mm. In addition, this maximum error is exclusively located in the closed configuration of the hand where the MoCap acquisitions are more difficult and less precise.** The second step is focused on the phalanx trajectories estimated by the  $TH_1$  hand dynamic model starting from the  $TH_2$  articulation angular variables (obtained through the inverse kinematic model of the  $TH_2$  trajectories). **In Fig. 8, the phalanx trajectories, called virtual phalanx trajectories, for the index finger both in the opening and closing gestures are depicted. It is worth noting that these trajectories are an approximation to a realistic grasping movement based on a multibody model and might not represent the real  $TH_1$  phalanx trajectories. These virtual phalanx trajectories are needed because the subject is not able to autonomously open and close his hands and it will be important in the final assessment of the HES system to assess the performance of the device to not alter the natural hand movement. This aspect leads to a qualitative evaluation of the ergonomics of the device.**

## 4. Exoskeleton model

In this chapter, the proposed 1 DOF mechanism for the exoskeleton fingers is presented and analysed. The results obtained in the previous part are used to determine the most suitable mechanism configuration, taking into account also the limitations in terms of encumbrances. This section is organized as follows, maintaining the same structure of the previous one:

- Data acquisition: the mechanism has been designed **for the two subjects** ( $TH_1$  and  $TH_2$ , characterized by different finger characteristics, see Tables 1-2). All the geometrical parameters are reported for

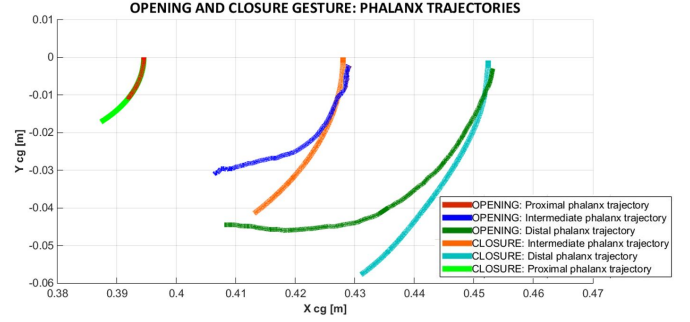


Figure 8:  $TH_1$  subject: virtual phalanx trajectories for the index finger during **both the opening and the closing phases**, reproduced starting from the  $TH_2$  articulation angular variables

**both subjects.** The same MoCap system is used to obtain the real mechanism trajectories. In particular, the authors focus their attention on five key points of the mechanism (Fig. 9 - 10).

- Kinematic model: a complete kinematic synthesis has been performed to obtain a suitable mechanism able to accurately follow the real fingers trajectories. The proposed mechanism kinematics can be easily written in a closed form and has a single DOF. The mechanism is adaptable to different hand sizes with a few variations of its geometrical parameters.
- Dynamic model: the authors have developed a 3D dynamic model of the hand exoskeleton. The dynamic model consists of different subsystems: the multi-body model, the cable and actuators models and the joint limit models. The subsystems interact to each other to simulate the dynamic behaviour of the whole mechanism. As clearly visible in Fig. 15, the same 1 DOF mechanism has been developed for each finger. The cable models (rigid wire) allow the calculation of the force acting on the bodies, neglecting, for sake of simplicity, the friction forces; this way, the tension is transmitted from the actuators to the end-effector of the mechanism. The joint limit models simulate the real exoskeleton behaviour by constraining the revolute-prismatic joints to work within a limited range (upper and lower bounds).
- Simulation results and experimental data: in this part, a comparison between the mechanism simulation results and the experimental data acquired through the MoCap system is shown (Fig. 16). For the sake of simplicity, the graphic shows the results only for the index finger of the  $TH_1$  mechanism. Given that the mechanism is based on the same architecture, the same results are also obtained for the other fingers and for the  $TH_2$  mechanism. In conclusion, the errors in terms of simulated and real key points trajectories are very satisfactory, confirming the reliable dynamic behaviour of the mechanism dynamic model.

The exoskeleton model acquisition and validation through the MoCap system are shown in the 2nd step of the video.

#### 4.1. Exoskeleton model: data acquisition

The single DOF mechanism is shown in Fig. 9 and consists of a kinematic chain mechanism able to perform the desired roto-translation of the end effector (point E in Fig. 9). The connection point between hand and exoskeleton is the intermediate phalanx; eventually, also the distal phalanx can be connected through a thimble (maintaining the same kinematics). Furthermore, the mechanism has a simple direct kinematics which only depends on the angle between the horizontal line and the distal phalanx  $\alpha_2$  (see Fig. 9). In Fig. 10, the same MoCap system has been

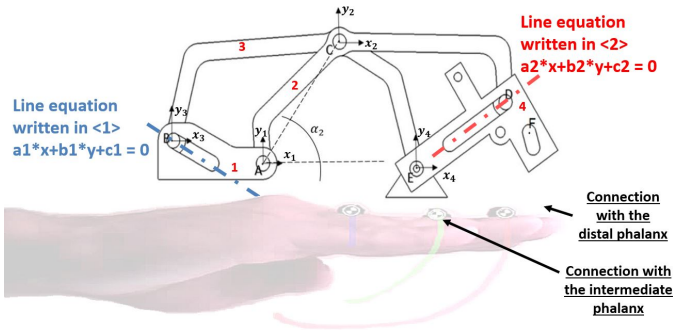


Figure 9: Description of the exoskeleton mechanism. Markers are the green points

used to acquire the data coming from the real prototype of exoskeleton to validate the dynamic model of the system during the **opening and closing gestures**. Since the mechanism is the same for all the fingers and it consists of rigid bodies, the comparison between real data and simulated trajectories is easier than in the case of the hand model; for these reasons, the trajectory acquisitions have been represented only for the index finger mechanism. In this case, the markers are placed in five key points of the mechanism (see the green points in Fig. 9, A-B-C-D-E). In addition, in order to simplify the kinematic and the

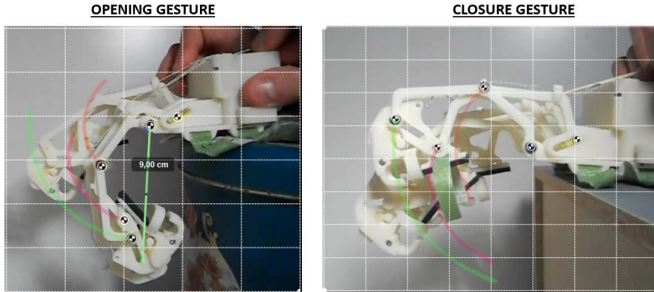


Figure 10: Experimental setup for the MoCap acquisitions of the  $TH_1$  exoskeleton

dynamic analyses, simplified geometries for the different parts have been adopted. These parts are related, for example, to the  $TH_1$  subject and described in Fig. 11. The

exoskeleton characteristics for  $TH_1$  and  $TH_2$  are respectively reported in Table 3 and Table 4, which contain the geometrical parameters of each part of the finger for the  $TH_1$  and the  $TH_2$  cases. The geometrical parameters are also shown in Fig. 11.

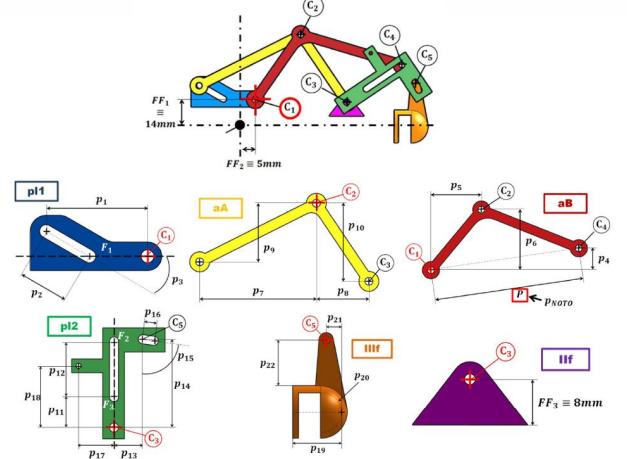


Figure 11: Exoskeleton mechanism parts

#### 4.2. Exoskeleton model: kinematic model

The kinematic model of the exoskeleton is developed to better analyze the mechanism parts trajectories. In the following section, to simplify the analytical description, the attention is focused only on the index finger trajectories, but the same model and the same approach have been adopted for all the fingers of both the  $TH_1$  and the  $TH_2$  subjects.

Fig. 9 shows the center of the reference system  $\langle 1 \rangle$  related to the body 1 fixed to the hand (point A). The other reference systems  $\langle 2 \rangle$ ,  $\langle 3 \rangle$ ,  $\langle 4 \rangle$  related to the bodies 2, 3, 4 are coincident, respectively, with points C, B and E (Fig. 9). The kinematic equations describing the mechanism are obtained starting from the revolute constraints in the points A, C and E:

$${}^0\underline{0} = {}^1\underline{C} + R_2^1(\alpha_2) {}^2\underline{A} \quad (3)$$

$${}^1\underline{C} = {}^1\underline{B} + R_3^1(\alpha_3) {}^3\underline{C} \quad (4)$$

$${}^1\underline{B} + R_3^1(\alpha_3) {}^3\underline{E} = {}^1\underline{E}. \quad (5)$$

Moreover, by analysing the two mechanical guides related to the points B and D, the equations of the constraints become:

$$a_1 \cdot {}^1B_x + b_1 \cdot {}^1B_y + c_1 = 0 \quad (6)$$

$$a_2 \cdot {}^4D_x + b_2 \cdot {}^4D_y + c_2 = 0 \quad (7)$$

$${}^1\underline{D} = {}^1\underline{C} + R_2^1(\alpha_2) {}^2\underline{D} \quad (8)$$

Table 3:  $TH_1$  exoskeleton characteristics [mm]

Finger	pl1 [ $p_1..p_3$ ]	aB [ $p_4..p_6$ ]	aA [ $p_7..p_{10}$ ]	pl2 [ $p_{11}..p_{18}$ ]	III f [ $p_{19}..p_{22}$ ]
Little	[23.9, 11.8, 30°]	[9.6, 25, 22, 65.4]	[44, 19.9, 22, 29.4]	[10.3, 18.4, 9.6, 29.4, 82°, 3.7, 11.8, 20.6]	[8.8, 5.1, 5.1, 12]
Ring	[32.5, 16, 30°]	[13, 36, 30, 89]	[60, 27, 30, 40]	[14, 25, 13, 40, 82°, 5, 16, 28]	[12, 7, 7, 16.5]
Middle	[34.7, 17, 30°]	[13.9, 38.4, 32, 95]	[64, 28.8, 32, 42.7]	[14.9, 26.7, 13.9, 42.7, 82°, 5.33, 17, 30]	[12.8, 7.5, 7.5, 17.6]
Index	[30.7, 15.1, 30°]	[12.3, 34, 28.3, 84]	[56.7, 25.5, 28.3, 37.8]	[13.2, 23.6, 12.3, 37.8, 82°, 4.7, 15.1, 26.4]	[11.3, 6.6, 6.6, 15.5]

Table 4:  $TH_2$  exoskeleton characteristics [mm]

Finger	pl1 [ $p_1..p_3$ ]	aB [ $p_4..p_6$ ]	aA [ $p_7..p_{10}$ ]	pl2 [ $p_{11}..p_{18}$ ]	III f [ $p_{19}..p_{22}$ ]
Little	[23.2, 11.5, 30°]	[9.4, 24.5, 21.7, 65.1]	[43.5, 19.4, 21.8, 28.9]	[10.1, 18.1, 9.3, 28.8, 79°, 3.4, 11.4, 20.2]	[8.5, 4.9, 4.9, 11]
Ring	[32.4, 15.8, 30°]	[12.8, 35.4, 29.8, 88.5]	[59.2, 26.6, 29.4, 41]	[13.8, 23.2, 11.5, 39.5, 82°, 4.5, 15.5, 27.7]	[11.7, 6.6, 6.6, 16.3]
Middle	[33.9, 16.5, 30°]	[14, 39, 31.5, 94.8]	[63.6, 28, 31.4, 42]	[14.1, 26, 13, 41.6, 82°, 6.1, 16.8, 29.1]	[12, 6.9, 6.9, 17]
Index	[30, 14.3, 30°]	[11.4, 33.1, 28, 83.5]	[56, 24.5, 27.6, 36.7]	[12.2, 23, 11.8, 36.7, 82°, 4, 14.3, 26]	[10.5, 5.7, 5.7, 14.5]

state vector  $\underline{q}$ :

$${}^1\underline{D} = {}^1\underline{E} + R_4^1(\alpha_4) {}^4\underline{D}. \quad (9)$$

The unknowns representing the state of the system  ${}^1\underline{C}$ ,  ${}^1\underline{B}$ ,  ${}^1\underline{E}$ ,  $\alpha_2$ ,  $\alpha_3$ ,  $\alpha_4$  can be calculated as a function of only  $\alpha_2$  by solving Eq. 3-9. The state vector is defined as follow:

$$\underline{q} = [{}^1\underline{B}^T; \alpha_2; {}^1\underline{C}^T; \alpha_3; {}^1\underline{E}^T; \alpha_4]^T, \in \mathbb{R}^9. \quad (10)$$

All the interesting points of the mechanism (included in the state vector  $\underline{q}$ ) are completely described as a function of the angle  $\alpha_2$  and of the geometrical parameters  $\underline{R} \in \mathbb{R}^{16}$ :

$$\underline{R} = ({}^2\underline{A}^T, {}^3\underline{C}^T, {}^2\underline{D}^T, {}^3\underline{E}^T, {}^4\underline{F}^T, a_1, b_1, c_1, a_2, b_2, c_2)^T, \quad (11)$$

where  ${}^2\underline{A}$  is (the point A) written in  $\langle 2 \rangle$ ,  ${}^3\underline{C}$  is (the point C) written in  $\langle 3 \rangle$ ,  ${}^2\underline{D}$  is (the point D) written in  $\langle 2 \rangle$ ,  ${}^3\underline{E}$  is (the point E) written in  $\langle 3 \rangle$ ,  ${}^4\underline{F}$  is (the point F) written in  $\langle 4 \rangle$  and  $a_1, b_1, c_1$  and  $a_2, b_2, c_2$  are the line equation coefficients (respectively written in the reference frames  $\langle 1 \rangle$  and  $\langle 4 \rangle$ ) of the mechanism linear constraints, highlighted in Fig. 9. All these parameters are completely known because they represent geometric quantities, depending only on the design of the exoskeleton parts and can be used to adapt the exoskeleton to different hand sizes. Consequently, it is possible to write the direct kinematic model  $\tilde{\underline{q}} = \underline{f}(\alpha_2, \underline{R}) \in \mathbb{R}^8$  (see Eq. 12) as a function of  $\alpha_2$  and  $\underline{R}$  where  $\tilde{\underline{q}}$  is the unknown part of the

$$\tilde{\underline{q}} = \begin{bmatrix} {}^1B_x \\ {}^1B_y \\ {}^1C_x \\ {}^1C_y \\ \alpha_3 \\ {}^1E_x \\ {}^1E_y \\ \alpha_4 \end{bmatrix} = \underline{f}(\alpha_2, \underline{R}). \quad (12)$$

The methodology to optimize the mechanism of each finger varying the geometrical parameters  $\underline{R}$  (Eq. 11) and to satisfy the encumbrance constraints is the following: starting from the acquired trajectories of the intermediate (and eventually also the distal phalanges), an optimization algorithm based on the minimization of a constrained nonlinear multivariable function [36], [37] aims at modifying the geometrical parameters to lead the mechanism to fit the acquired trajectories. The objective function of the algorithms minimizes the error between the acquired trajectories (used as the reference ones) and the same trajectories obtained through the exoskeleton mechanism. The optimization algorithm requires suitable upper and lower bounds for the model parameters to find out a correct solution for the kinematics, respectively stated as  $\underline{U}_b, \in \mathbb{R}^{16}$  and  $\underline{L}_b, \in \mathbb{R}^{16}$ .

To generalize the methodology, **both the intermediate and the distal phalanges** are implemented. Defining the desired experimental angular variable  $\alpha_2(t)$  in the discrete range  $t \in [t_0, t_1, ..t_i..t_N]$  for  $i = 1, 2, ..., N$  (acquired by the MoCap system), the XY plane trajectories for the intermediate and distal phalanges can be written as:

$$\hat{\underline{q}}_{des}(t) = [x_{inter}(t), y_{inter}(t), x_{dist}(t), y_{dist}(t)]^T \in \mathbb{R}^4. \quad (13)$$

Considering the same angular variable  $\alpha_2(t)$  also for the simulated system, the kinematic model provides the simulated trajectories,  $\hat{\underline{q}}_{sim} = \hat{\underline{q}}_{sim}(\alpha_2, \underline{R}) \in \mathbb{R}^4$ :

$$\hat{\underline{q}}_{sim}(\alpha_2(t), \underline{R}) = [{}^1E_x(\alpha_2, \underline{R}), {}^1E_y(\alpha_2, \underline{R}), {}^1F_x(\alpha_2, \underline{R}), {}^1F_y(\alpha_2, \underline{R})]^T. \quad (14)$$

The objective function is a scalar function  $F(\underline{R})$  equal to the Euclidean 2-norm of the errors between  $\hat{\underline{q}}_{des}(t)$  and  $\hat{\underline{q}}_{sim}(\alpha_2(t), \underline{R})$ :

$$F(\underline{R}) = \left\| \hat{\underline{q}}_{des} - \hat{\underline{q}}_{sim} \right\|_2^2 = \sum_{i=1}^N \left\| \hat{\underline{q}}_{des}(t_i) - \hat{\underline{q}}_{sim}(\alpha_2(t_i), \underline{R}) \right\|_2^2. \quad (15)$$

The optimization algorithm has to minimize the error to follow the desired phalanx trajectories  $\hat{\underline{q}}(t)_{des}$  taking into account the following non linear constraints:

$$\begin{aligned} & \left\| \hat{\underline{q}}_{des}(t) - \hat{\underline{q}}_{sim}(\alpha_2(t), \underline{R}) \right\|_\infty = \\ & = \max_i \left\| \hat{\underline{q}}_{des}(t_i) - \hat{\underline{q}}_{sim}(\alpha_2(t_i), \underline{R}) \right\|_\infty \leq C. \end{aligned} \quad (16)$$

where the  $\infty$ -norm is needed to maintain limited the maximum error and  $C$  is the threshold value. Since the mechanism has to be also optimized in terms of encumbrances (especially, for the height of the point  ${}^1\underline{C} = [{}^1C_x(\alpha_2, \underline{R}), {}^1C_y(\alpha_2, \underline{R})]^T$ ), a non linear constraint on this point is introduced:

$$\max_i ({}^1C_y(\alpha_2(t_i), \underline{R}) - h({}^1C_x(\alpha_2(t_i), \underline{R}))) \leq 0 \quad (17)$$

where  $y = h(x)$  is the non linear function of the constraint

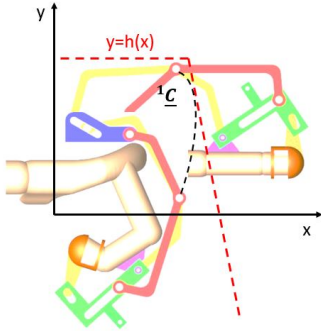


Figure 12: Encumbrance constraint **obtained forcing the point C to remain lower than the constraint**

for point  ${}^1\underline{C}$  point (Fig. 12) which is necessary to model the vertical encumbrance.

The minimization problem is completely described by the following equation:

$$\min_{\underline{R}} F(\underline{R}) : \begin{cases} \underline{L}_b \leq \underline{R} \leq \underline{U}_b \\ \max_i \left\| \hat{\underline{q}}_{des}(t_i) - \hat{\underline{q}}_{sim}(\alpha_2(t_i), \underline{R}) \right\|_\infty \leq C \end{cases} \quad (18)$$

$$\max_i ({}^1C_y(\alpha_2(t_i), \underline{R}) - h({}^1C_x(\alpha_2(t_i), \underline{R}))) \leq 0. \quad (19)$$

The optimization algorithm employed to solve the problem is the ‘trust region reflective’ algorithm, applied exploiting the knowledge of the gradient of the  $F(\underline{R})$  function [36].

#### 4.3. Exoskeleton model: dynamic model

After the kinematic model, a complete 3D dynamic model of the exoskeleton has been developed. To perform a realistic simulation of the exoskeleton, different submodels are implemented:

- **Multibody model:** as clearly visible in Fig. 15, the same 1 DOF mechanism has been developed for each finger. The multibody model consists of different parts: the fixed part (a) (blue) has two joints (1 fixed revolute and 1 mobile revolute-prismatic) which connect (a) with the yellow link (b) and the red one (c). The yellow and the red links are connected together through a fixed revolute joint. The green body (d), as the end-effector of the mechanism, is linked by two joints, i.e. 1 fixed revolute joint and 1 mobile revolute-prismatic one. The cable tensions act on the green part to actuate the mechanism. Finally, the orange part (e) is constrained to the green body by means of 1 mobile revolute-prismatic joint. The orange part (the thimble) is introduced to improve the ergonomics of the exoskeleton by moving also the distal phalanx during the hand opening, but the end-effector of the mechanism remains always the green body. In fact, the connection between the distal phalanx and the thimble is optional, because it does not alter the kinematic model of the mechanism. As regards the description of the bodies and of the joints, the geometry, the masses and the inertias are directly provided by 3D CAD evaluations. The inputs of this model are the cable tensions produced by the cable and actuator models, the reaction forces calculated by the joint limit models and the external interactions due to the hand model (simulated through a 3D bushing constrain). The outputs are the exoskeleton motion and the reaction forces applied on the hand model.

- **Joint Limit models:** these models (see Fig. 13) simulate the real exoskeleton behaviour by constraining the revolute-prismatic joints to act within a specific range (upper and lower bounds). The physical limits of the joint movement are modelled through the application of proper reaction forces between the two moving bodies; in particular, the value of the force will depend upon the position  $d_i$  of the part inside the prismatic guide through a non-linear law (shown in Fig. 13). The inputs are the joint linear coordinates  $d_i$  and the outputs are the reaction forces  $F_i$ . In Fig. 13, the non-linear behaviour of the reaction forces is displayed, where  $F$  is the force value applied along the direction of the guide between the two bodies,  $l_L$  and  $l_U$  are the lower and upper limits of the guide,  $k_0$  is the gap and  $F_{MAX}$  is the maximum value of the force.

- **Cable and actuator models:** these models (Fig. 14) allow the calculation of the cable forces on the

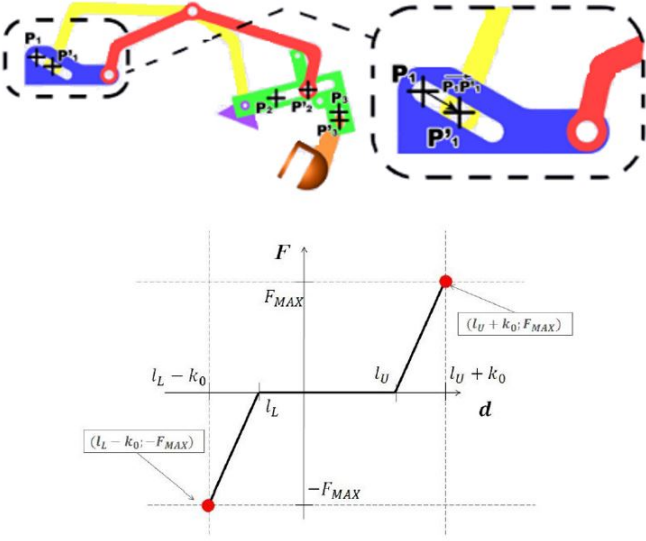


Figure 13: Joint limit submodel: (a) force law (b) application of the force law on the mechanism

bodies, neglecting the friction forces. The proposed HES is controlled in terms of desired actuator speed (kinematic control of the mechanism) and the length of the cable is a function of the mechanism configuration (see Fig. 14-15). The mechanism has a pre-

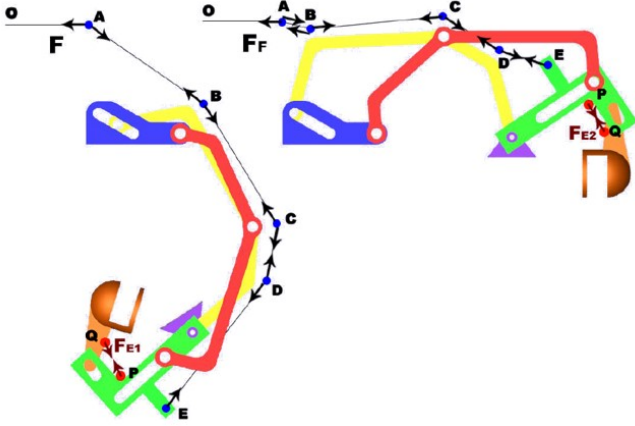


Figure 14: Cable submodel: tension transmission

defined passage for the cable, therefore the mechanism configuration and the cable length are related through only one solution  $L(\alpha_2)$ . The cable tension is transmitted from the actuators to the multibody model (the end-effector of the mechanism, the green bodies (d)). In particular, **by supposing the cable tension is conserved and the wire is rigid**, the actuation model produces a torque proportional to the velocity error between the desired wire velocity  $v_m = \theta_m r$  (where  $\theta_m$  is the motor speed and  $r$  is the pulley radius) and the real wire velocity  $v_e$ . **Supposing a known motor speed  $\theta_m$  and type**, the torques and the cable tension applied to the multi-

body model are simply determined by the configuration (because the cable tension directions are supposed to be known). The model inputs are the desired actuator velocities and the joint angular coordinates; the outputs are the cable tensions calculated by knowing the mechanism configuration and the speed error of the controller.

#### 4.4. Exoskeleton model: simulation results and experimental data

In this section, a comparison between the real mechanism trajectories acquired by the MoCap system and the simulated trajectories has been presented, for example, for the  $TH_1$ . Since the mechanism is the same for all the fingers, the results are shown only for the index finger of the  $TH_1$ . Similar results are obtained also for the  $TH_2$  mechanism, but for sake of synthesis are not here reported. In Fig. 16 the comparisons between the exoskeleton model trajectories and the experimental data are shown for the A, B, C, D and E points. The errors are very small, less than 2 mm, mainly due to the camera acquisition misalignment and to the model approximations.

## 5. Hand Exoskeleton System

In this chapter, the whole hand exoskeleton model and prototype will be presented; in particular, the description of the complete dynamic model (obtained by coupling together the hand and the exoskeleton models), the study of the prototype design phases and the analysis of the experimental results will be discussed in details. Both for the  $TH_1$  and for the  $TH_2$  subjects, the HES validations are respectively shown in the 3rd-4th steps of the video.

### 5.1. Hand exoskeleton system: dynamic model

The complete hand exoskeleton model is obtained by coupling together **the hand and the exoskeleton models**. As described before, the exoskeleton is studied to be **a single phalanx mechanism (1 DOF of the finger mechanism is actuated by 1 actuator)**, but for sake of ergonomics, also the distal phalanx is connected to the mechanism. However, the connection of the distal phalanx through a thimble does not alter the kinematic model of the mechanism because **it remains the same single DOF mechanism**. In fact, by adding the thimble the mechanism adds 1 body with 3 DOFs but the kinematic chain of the finger adds 1 DOF, thus the finger+mechanism kinematic chain maintains the same 1 DOF (the controlling DOF is  $\alpha_2$ ). In addition, the connection points between phalanges and mechanism introduce some compliance effects in order to keep the hand safe and to absorb the minimal variations due to the hands geometry. Nevertheless, it is worth nothing that this compliance does not affect the exoskeleton functionality.

As regards the dynamic model, the linking between

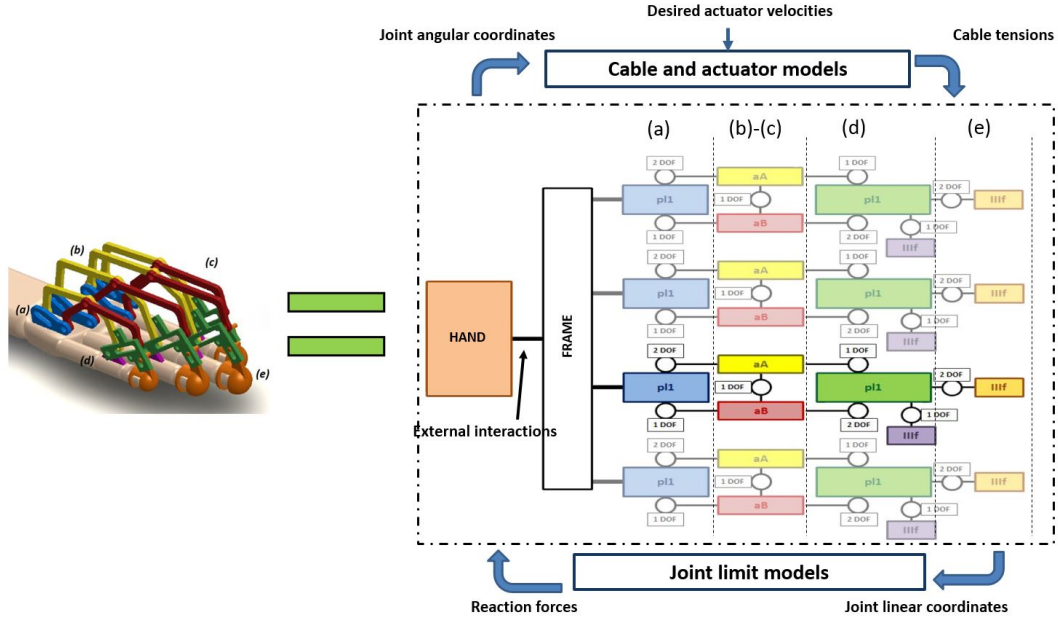


Figure 15: Architecture of the exoskeleton model

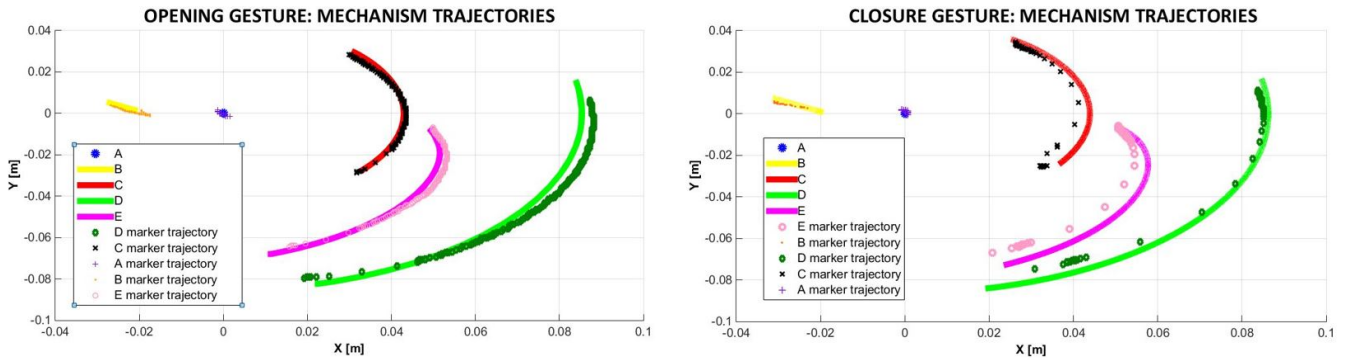


Figure 16: Comparison between the  $TH_1$  exoskeleton model trajectories and the real ones for the index finger during both the **opening** and the **closing** gestures

these two models is simulated through two 3D force elements between fingers and the exoskeleton mechanism. As visible in Fig. 17, the interaction points are placed in the intermediate phalanx and in the distal one. The complete model allows the simulation of both ‘**hand closing**’ and ‘**hand opening**’ gestures (as shown in Par. 3.1 in Fig. 4). The ‘**hand closing**’ simulation mode is very useful to analyse the kinematic behaviour of the whole HES model (because the hand drives the exoskeleton motion); instead, the ‘**hand opening**’ simulation mode is needed to evaluate the cable tensions able to extend the fingers by using the exoskeleton mechanism. In both cases, the complete hand exoskeleton model is important to study the forces exchanged between the hand and the exoskeleton (on the hand back and on the phalanges). The complete model allows the simulation of the classical ‘**hand closing**’ and ‘**hand opening**’ gestures. The ‘**hand closing**’ simulation mode is very useful

to analyse the kinematic behaviour of the whole HES model (because the hand drives the exoskeleton motion); instead, the ‘hand opening’ simulation mode is needed to evaluate the cable tensions able to extend the fingers by using the exoskeleton mechanism. In both cases, the complete hand exoskeleton model is important to study the forces exchanged between the hand and the exoskeleton (on the hand back and on the phalanges).

### 5.2. Hand exoskeleton system: prototype design

According to the requirements and the model results obtained in the previous parts, the real prototype of the HES is developed. The HES prototype consists of two main parts: the mechanism and the actuation system with the control unit (for instance, for **the  $TH_1$  subject**). The mechanism has been built up by using a 3D printing machine in a thermoplastic polymer, Acrylonitrile Butadiene

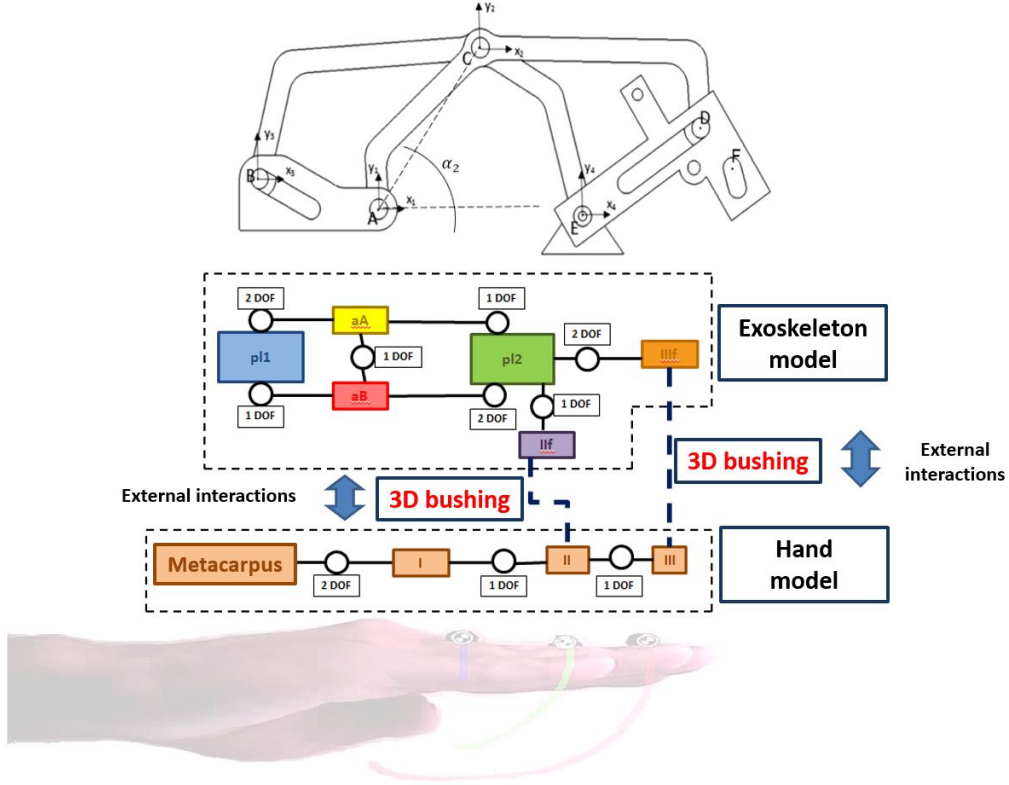


Figure 17: HES dynamic model

Styrene (ABS), which has sufficient mechanical resistance and stiffness.

### 5.2.1. Mechanism design

During the design phase of the mechanism, mainly due to the passage from the simplified model (based on the mechanism parts described in Fig. 11) to the real hand exoskeleton parts (designed for all the fingers), some important key issues have been faced: in particular, the mechanism has been re-designed starting from the simplified model used in the previous chapters but maintaining the same kinematics. In fact, the re-designed mechanism, compared to the simplified one, is more stable because the  $aB$  part (Fig. 18) has been modified to obtain a symmetric configuration. In particular, the symmetric configuration does not change the mechanism trajectories, but it requires the splitting of the  $aB$  part into two parts (duplication of the  $aB$  part). Nevertheless, the introduction of the symmetric configuration of the  $aB$  part has led to some problems in terms of lateral encumbrances; for this reason, to reduce the lateral encumbrances of each finger mechanism, all the pins are integrated with the lateral rods as clearly visible in the  $aA$  and  $aB$  parts (Fig. 18). Since the hand exoskeleton systems for the  $TH_1$  subject and for the  $TH_2$  subject are quite different, two prototypes have been designed: in Tables 5 - 6, all the geometrical characteristics of the mechanism parts (both for the  $TH_1$  and  $TH_2$  subjects) are described in terms of length  $l_p$ , height  $h_p$  and lateral size  $l_{s_p}$  (for example, for the  $TH_1$  subject, see Fig.

18).

Table 5:  $TH_1$  subject: mechanism characteristics for each finger [cm]

	Index [ $l_p, h_p$ ]	Medium [ $l_p, h_p$ ]	Ring [ $l_p, h_p$ ]	Small [ $l_p, h_p$ ]
aA	[7.5, 3.5]	[8.4, 4.8]	[6.9, 3.6]	[5.5, 2.7]
aB	[7.6, 3.5]	[8.2, 4.8]	[7, 3.6]	[5.5, 2.7]
p11	[3.5, 1.2]	[4, 1.5]	[3.5, 1.2]	[2.5, 1.2]
p12	[4, 5.2]	[5, 6.4]	[3.8, 5.1]	[3.1, 4]
Total	[12, 4.2]	[13, 5]	[11.5, 4.1]	[9, 3]

In Fig. 18 the whole 3D CAD model of the mechanism is shown for the  $TH_1$  subject; as clearly visible, both the lateral encumbrances and the vertical ones are very limited.

### 5.2.2. Actuation system and control unit

The actuation system and the control unit are developed under a low cost concept; therefore, many solutions that can be found in the state of the art have been avoided due to their higher costs [38], [29], [39]. In addition, since the reduction of the total masses is a strict requirement, high power density actuators for the direct implementation on the hand have been chosen. The requirements for the selected motors (Savox  $SH - 0254$ ) are obtained from the simulation results: they have a maximum torque of

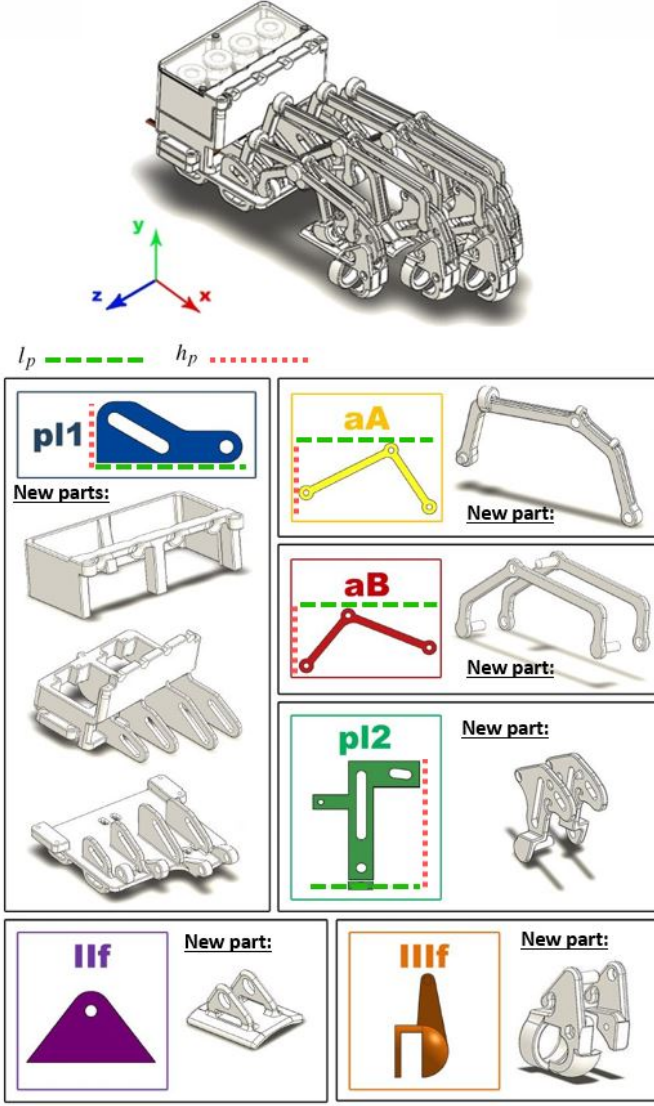


Figure 18: HES 3D model: re-design process of the exoskeleton parts

3.1 kg\*cm @4.8 V and 3.9 kg\*cm @6.0 V with a size of 22.8x12x29.4 mm (**l\*w\*h**) and weight of 16 g. The maximum angular speed is 6.25 rad/s @4.8 V and 7.69 rad/s @6.0 V. Some experimental tests performed on these servomotors confirm their characteristics and their capacity to easily actuate the exoskeleton.

**Regarding** the control unit, the device is a MicroMaestro control board able to manage up to 6 servomotors or control sensors with a limited encumbrances (**21 mm length x 30 width mm** and a weight of 5 g). The control architecture is based on a kinematic control of the motor speed (PID control) and it is directly controlled **by the subject** who uses two buttons for the opening and for the closing phases. The final electronic board contains the MicroMaestro device, two buttons for the control and one switch for the electric feed. The battery is a compact 4-cell Lithium battery (@6.0 V).

Concerning the software part, the MicroMaestro device al-

Table 6:  $TH_2$  subject: mechanism characteristics for each finger [cm]

	Index [ $l_p, h_p$ ]	Medium [ $l_p, h_p$ ]	Ring [ $l_p, h_p$ ]	Small [ $l_p, h_p$ ]
aA	[7.3,3.2]	[8.1,4.6]	[6.7,3.2]	[5.1,2.4]
aB	[7.4,3.4]	[8,4.7]	[7.2,3.4]	[5.1,2.3]
pl1	[3.3,1.1]	[3.8,1.3]	[3.4,1.1]	[2.3,1.1]
pl2	[3.7,4.8]	[5.1,5.8]	[3.5,4.9]	[2.9,3.8]
Total	[11.6,4]	[12.5,4.5]	[1.5,3.9]	[8.8,2.9]

lows the storing of scripts directly on the chipset memory. As described before, the control strategy aims at tracking a desired motor velocity  $\theta_m$  which is directly related to the mechanism speed  $\dot{\alpha}_2$  due to the characteristics of the kinematics. A mean value of the opening velocity for each finger is considered in terms of  $\dot{\alpha}_2$ ; **to achieve** a simultaneous opening of all the fingers in a predefined time (2.5 s), different values of the opening velocities had to be calculated.

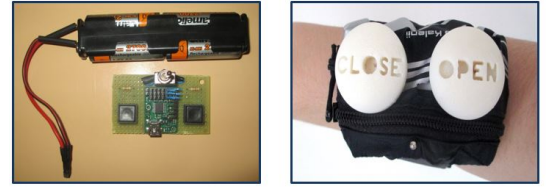


Figure 19: Actuation system and control unit

### 5.3. Hand exoskeleton system: numerical results and validation

**The hand and the exoskeleton models** have been integrated together to perform numerical simulations of the whole system. In addition, several acquisitions of the hand exoskeleton prototype have been performed both for the  $TH_1$  and the  $TH_2$  subjects during **opening and closing phases**. The main objectives of this part are:

- Trajectories comparison between the simulated and the experimental hand exoskeleton systems, both for the  $TH_1$  and for the  $TH_2$  subjects. This way, the hand exoskeleton dynamic model will be validated.
- Exoskeleton effectiveness in reproducing the desired real phalanx trajectories. This analysis is obtained by means of the comparison between the experimental phalanx trajectories acquired during free hand movements and the same ones provided by the exoskeleton prototype (hand exoskeleton system). The results will be useful to understand the transparency of the HES. The comparison for the  $TH_2$  subject will be carried out between the hand acquisition shown in Fig. 7 and the new acquisitions with the HES. Concerning the  $TH_1$  subject, due to the lack of the real hand acquisitions, the results obtained by the virtual acquisition

campaign (shown in Fig. 8) will be compared to the acquisitions coming from the HES.

### 5.3.1. $TH_1$ subject results

In Fig. 20, the experimental setup for the MoCap acquisition both for phalanx markers and for the mechanism key points is shown. The MoCap markers were placed both on the exoskeleton mechanism and on the finger phalanges: five markers for the exoskeleton (points A, B, C, D and E) and three markers for the phalanges (set up in the middle points). The acquisitions have been performed according to the simulations, both during the opening and the closing phases. The movement has been simulated starting by the closed hand configuration to the open hand configuration, and viceversa. Fig. 21 shows the compar-

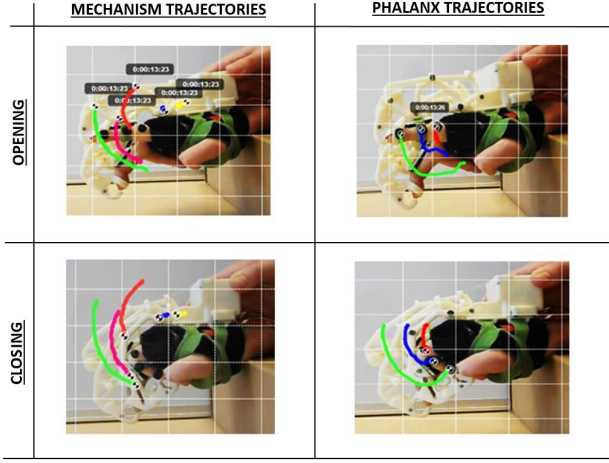


Figure 20: Experimental setup for the  $TH_1$  hand exoskeleton system validation. Markers are placed both on the phalanges and on the exoskeleton key points

ison between the trajectories obtained by the HES multibody model and trajectories acquired by the MoCap system (trajectories are shown for sake of simplicity for the index finger only). The trajectories are shown with respect to the world reference frame placed in the middle of the forearm. In this manner, it is possible to evaluate the capacity for the HES model to simulate the real device. As clearly visible from the figure, in both cases, the results are quite satisfactory in terms of trajectory matching: the real trajectories are tracked by the simulated ones, both for the exoskeleton mechanism and for the finger phalanges, despite of some unmodelled effects such as the compliance of the human tissues. The maximum errors are limited (8 mm max) and acceptable because they are mainly related to the closed hand configuration where the exoskeleton has the minimum effect on the hand and it is able to adjust its configuration to adapt it to the real hand gesture (improving the ergonomics

of the device). Moreover, these results mean that the multibody model is able to simulate the real behaviour of the hand coupled with the exoskeleton but, a more realistic contact model (including the compliance of the human tissue), is probably needed to simulate the closed hand configuration. In Fig. 22, the comparison between the virtual phalanx trajectories (shown in Fig. 8) and the real ones obtained with the complete HES during the same gestures is shown. Since the  $TH_1$  subject is not able to autonomously open his hands, a numerical simulation has been performed to obtain the virtual phalanx trajectories (calculated by applying the  $TH_2$  articulation angular variables to the hand model, please see Par. 3.4). This latter im-

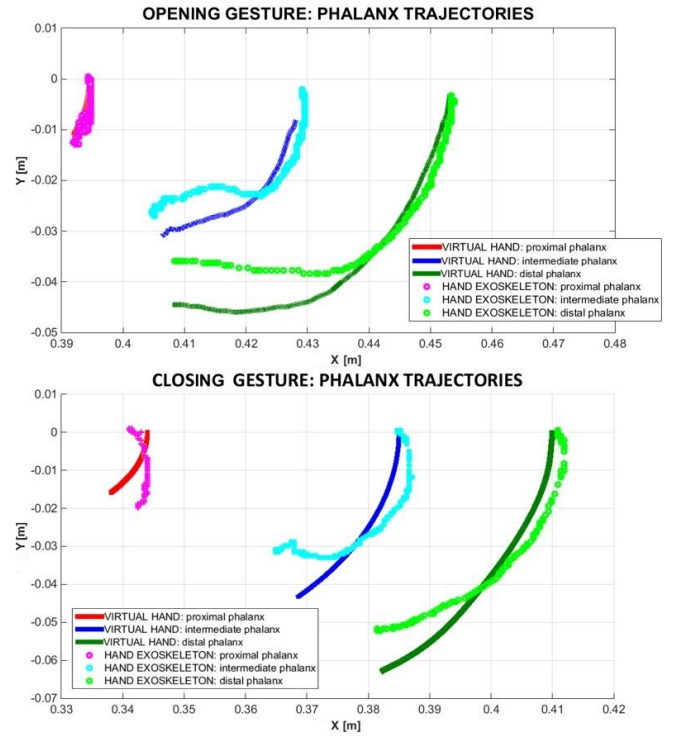


Figure 22:  $TH_1$  subject: comparison between the virtual phalanx trajectories and the real ones for the index finger

portant result, together with the positive feedback of the  $TH_1$  subject, indicates that the HES does not alter significantly the natural phalanx trajectories, during both phases. In Fig. 22, the limited errors measured in the closed hand configuration between the virtual and the real phalanx trajectories are mainly due to the difficulties to simulate the hand impairment of the  $TH_1$  subject, as mentioned in Par. 3.4.

### 5.3.2. $TH_2$ subject results

This section shows the results for the  $TH_2$  subject during some acquisitions performed with the HES prototype. In Fig. 23 the experimental setup for the MoCap acquisi-

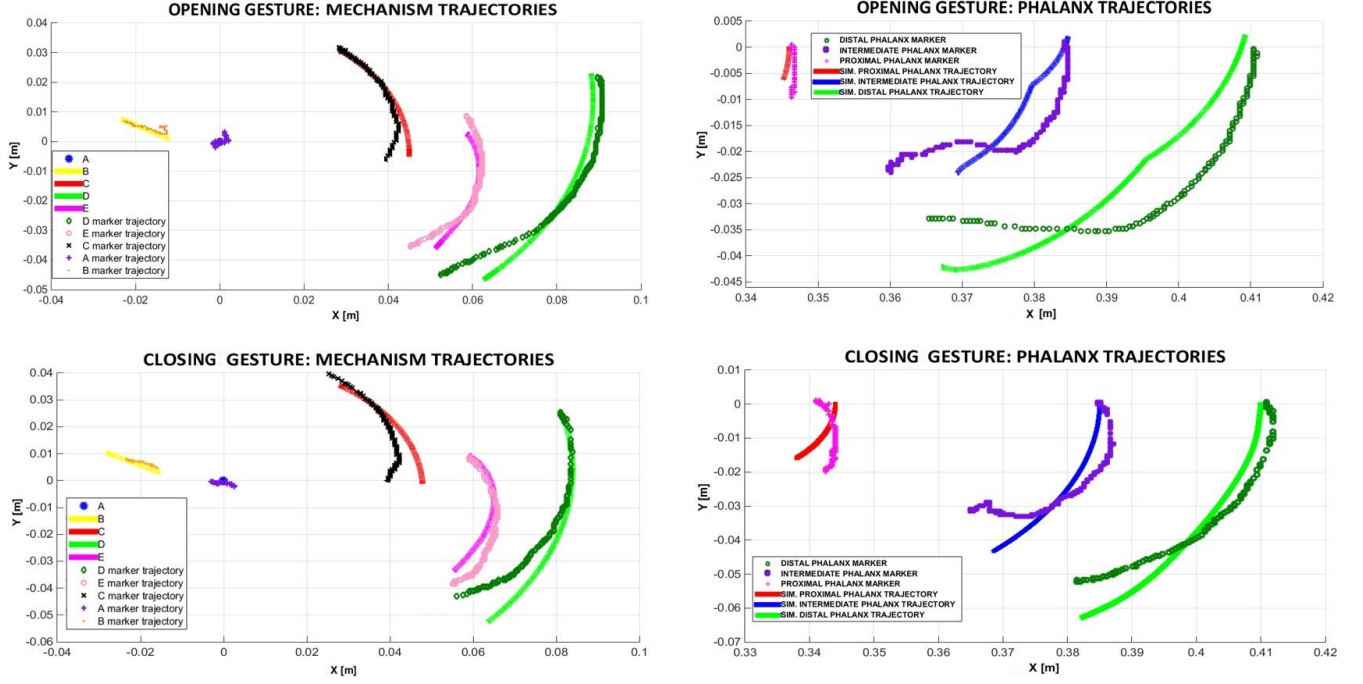


Figure 21:  $TH_1$  subject: comparison between the trajectories of the hand exoskeleton model and the trajectories acquired by the MoCap system of the real prototype for the index finger

tion both for phalanx markers and for the mechanism key points is reproduced. As in the previous case, the MoCap markers were placed both on the exoskeleton mechanism and on the finger phalanges and the acquisitions have been performed both during the opening and the closing phases. Fig. 24 shows the comparison between the

precisely than the  $TH_1$  subject. This is probably caused by the smoothness of the  $TH_2$  trajectories with respect to the  $TH_1$  ones. In fact, the  $TH_1$  subject has a hand deformation (see Fig. 3) which alters the normal trajectories for the opening and closing gestures. Finally, both for the exoskeleton mechanism and for the finger phalanges, the errors are quite small and they confirm the results obtained in the previous section (see Fig. 24). The comparison between the acquired and the simulated mechanism markers shows a maximum error of 8 mm in the closed hand configuration which is probably due to the different behaviour of the connection points between phalanges and mechanism. As described before for the  $TH_1$  subject, the multi-body model is able of simulating the dynamic behaviour of the hand exoskeleton system (see Par. 5.1) for the whole trajectory, but some unmodelled effects (compliance of human tissue and of the physical connection between the phalanx and the mechanism) are shown in the closed hand configuration. Finally, in Fig. 25 the comparison between the real phalanx trajectories (Fig. 4) and the same trajectories acquired by using the HES prototype is shown. Also in this case, this result points out that, during both phases, the HES does not modify the natural phalanx trajectories. It is worth noting the maximum error, about 5 mm, between the simulated and real trajectories mainly due to by the greater smoothness of  $TH_2$  trajectories compared to the  $TH_1$  ones.

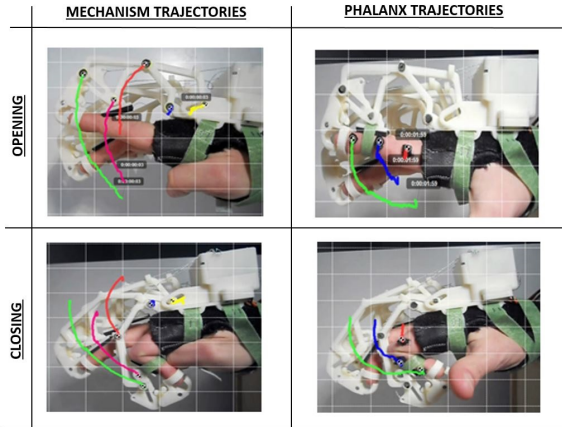


Figure 23: Experimental setup for the  $TH_2$  hand exoskeleton system validation. Markers are placed both on the phalanges and on the exoskeleton key points

trajectories of the hand exoskeleton model and the trajectories acquired by the MoCap system of the functional prototype, for the sake of synthesis, for the index finger only. The numerical results are very close to the real trajectories: the exoskeleton is able to follow the acquired trajectories more

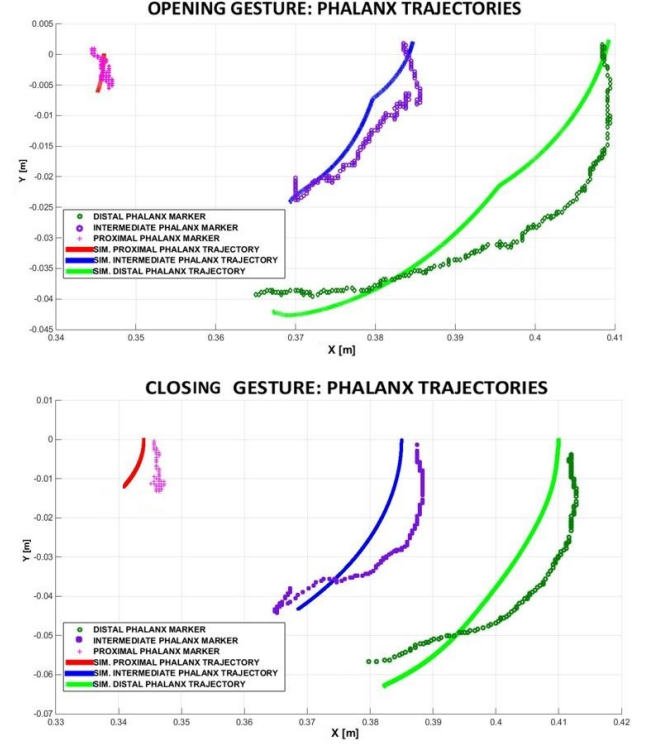
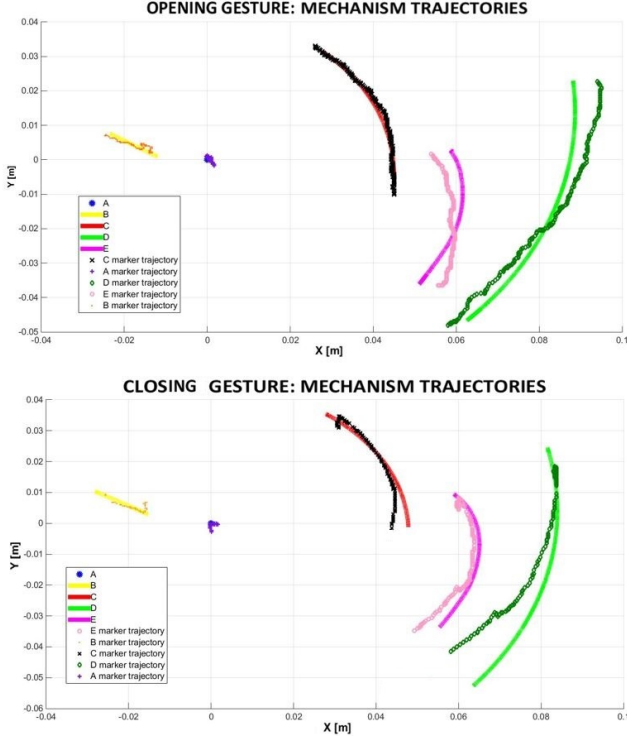


Figure 24:  $TH_2$  subject: comparison between the trajectories of the hand exoskeleton model and the trajectories acquired by the MoCap system of the real prototype for the index finger

## 6. Conclusion and further developments

In this work, the modelling, the development and the testing phases of a portable Hand Exoskeleton System for **hand-opening impairment** have been presented (see the attached video). Because of the strict requirements in terms of portability, adaptability and **affordability**, the main novelty of this HES is the 1 DOF mechanism (never used before in the hand exoskeleton field) able to precisely follow the desired phalanx movements, avoiding the problems related to the MetaCarpophalangeal self alignment. In addition, due to the characteristics of the kinematic chain (easily describable in closed form), a precise estimation of the mechanism configuration and a higher adaptability have been reached. High adaptability can be obtained only varying a few geometrical characteristics of the mechanism and a semi-automatic procedure based on optimization algorithms to adapt the mechanism to different hand sizes has been developed. Finally, thanks to the proposed architecture, both opening and closing gestures can be easily performed by obtaining good performance in terms of stiffness and forces. The achievement of a suitable mechanism for **the  $TH_1$  subject** has been obtained through a model-based approach: a complete 3D modelling of the hand and the exoskeleton (both validated through a MoCap system) has been implemented.

The MoCap acquisitions to validate the hand model have been performed on **the  $TH_2$  subject**, who is able to voluntarily open his hands. The  $TH_2$  phalanx trajectories are then used to extract the articulation angu-

lar variables through the inverse kinematic model of the hand. By means of the same articulation angular trajectories, some numerical simulations have been carried out also for the  $TH_1$  to replicate the same gestures. Consequently, basing on the results of the hand models, two different exoskeleton models (for the two subjects) have been firstly developed and then validated through the MoCap system. In fact, in parallel with this activity, a complete HES model (hand and exoskeleton models connected together) for the assessment of the kinematic and dynamic behaviour has been developed. After that, the kinematic validation has been made by comparing the results of the complete HES model and the acquisitions performed both on the mechanism markers and on the phalanges (for both subjects). *The results shown in Par. 5.3.1-5.3.2 indicate the capacity of the multi-body model to simulate a very complex situations for most of the trajectories. However, some unmodelled effects, probably caused by the human tissue compliance, affect the final part of the simulations (closed hand configuration), introducing a maximum error of 8 mm and 5 mm respectively for the two subjects (Fig. 21-22-24-25). Despite of these inaccuracies, the results depicted in Fig. 22-25 together with the feedback of the subjects, indicates that the HES is able to replicate the natural hand trajectories guaranteeing a comfortable*

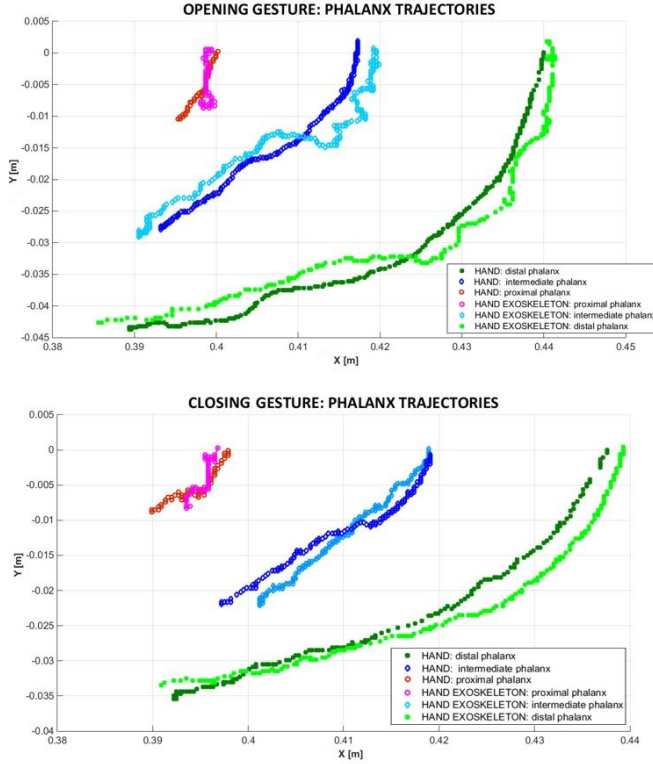


Figure 25:  $TH_2$  subject: comparison between the real phalanx trajectories and the same ones with the HES prototype for the index finger

*solutions during the opening and closing gestures. The authors have planned to introduce between the device and the hand back of the subjects a suitable force sensor able to estimate the pressure, and thus the real comfort, during the hand opening and closing. As regards the future developments, both this new*

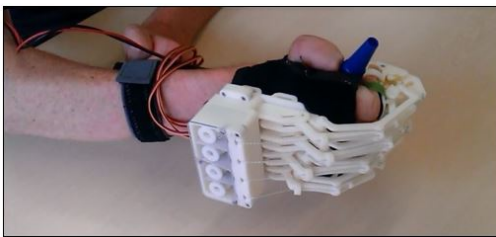


Figure 26: Testing phase of the  $TH_1$  HES prototype: grasping of a small object

*hand exoskeleton system and the model-based methodology (based on the real phalanx acquisitions and on optimization algorithms) will be tested soon on different subjects, through a collaboration with a rehabilitation center, aiming at the evaluation of the mechanism adaptability for other hand disabilities. It is also planned to study a new multi-body model of the HES and the proper kinematic architecture for the thumb to perform complete object grasping. Finally, some tests with different types of sensors and force controllers will be carried out.*

## ACKNOWLEDGMENT

A special thank goes to the Mechatronics and Dynamic Modelling Lab of the University of Florence, where the research activity has been carried out, and to the Italian National Research Council (CNR) - Institute for Complex Systems and in particular to Dr. M. Bianchini and Dr. B. Tiribilli for their support and assistance, and to Dr. S. Silvestri and Dr. D. Martelli, that have collaborated to the Hand Exoskeleton System development.

## References

- [1] W. Harwin, J. Patton, V. Edgerton, Challenges and opportunities for robot-mediated neurorehabilitation, Proceedings of the IEEE 94 (9) (2006) 1717–1726. doi:10.1109/JPROC.2006.880671.
- [2] L. Mertz, The next generation of exoskeletons: Lighter, cheaper devices are in the works, Pulse, IEEE 3 (4) (2012) 56–61. doi:10.1109/MPUL.2012.2196836.
- [3] B. Siciliano, O. Khatib, Springer Handbook of Robotics, Springer-Verlag Berlin Heidelberg, Berlin, Germany, 2008.
- [4] P. Heo, G. M. Gu, S. Lee, Current hand exoskeleton technologies for rehabilitation and assistive engineering, Int. J. Precis. Eng. Manuf. 13 (5) (2012) 807–824.
- [5] A. Schiele, F. van der Helm, Kinematic design to improve ergonomics in human machine interaction, Neural Systems and Rehabilitation Engineering, IEEE Transactions on 14 (4) (2006) 456–469. doi:10.1109/TNSRE.2006.881565.
- [6] R. Leeb, M. Gubler, M. Tavella, H. Miller, J. del Millan, On the road to a neuroprosthetic hand: A novel hand grasp orthosis based on functional electrical stimulation, in: Engineering in Medicine and Biology Society (EMBC), 2010 Annual International Conference of the IEEE, 2010, pp. 146–149. doi:10.1109/IEMBS.2010.5627412.
- [7] Y. Yihun, R. Miklos, A. Perez-Gracia, D. Reinkensmeyer, K. Denney, E. Wolbrecht, Single degree-of-freedom exoskeleton mechanism design for thumb rehabilitation, in: Engineering in Medicine and Biology Society (EMBC), 2012 Annual International Conference of the IEEE, 2012, pp. 1916–1920. doi:10.1109/EMBC.2012.6346328.
- [8] C. Jones, F. Wang, R. Morrison, N. Sarkar, D. Kamper, Design and development of the cable actuated finger exoskeleton for hand rehabilitation following stroke, Mechatronics, IEEE/ASME Transactions on 19 (1) (2014) 131–140. doi:10.1109/TMECH.2012.2224359.
- [9] B. Choi, H. Choi, Skk hand master-hand exoskeleton driven by ultrasonic motors, in: Intelligent Robots and Systems, 2000. (IROS 2000). Proceedings. 2000 IEEE/RSJ International Conference on, Vol. 2, 2000, pp. 1131–1136 vol.2. doi:10.1109/IROS.2000.893171.
- [10] M. DiCicco, L. Lucas, Y. Matsuoka, Comparison of control strategies for an emg controlled orthotic exoskeleton for the hand, in: Robotics and Automation, 2004. Proceedings. ICRA '04. 2004 IEEE International Conference on, Vol. 2, 2004, pp. 1622–1627 Vol.2. doi:10.1109/ROBOT.2004.1308056.
- [11] C. Jones, F. Wang, R. Morrison, N. Sarkar, D. Kamper, Design and development of the cable actuated finger exoskeleton for hand rehabilitation following stroke, Mechatronics, IEEE/ASME Transactions on 19 (1) (2014) 131–140. doi:10.1109/TMECH.2012.2224359.
- [12] J. Blake, H. Gurocak, Haptic glove with mr brakes for virtual reality, Mechatronics, IEEE/ASME Transactions on 14 (5) (2009) 606–615. doi:10.1109/TMECH.2008.2010934.
- [13] J. Iqbal, N. Tsagarakis, D. Caldwell, Human hand compatible underactuated exoskeleton robotic system, Electronics Letters 50 (7) (2014) 494–496. doi:10.1049/el.2014.0508.

- [14] A. Wege, K. Kondak, G. Hommel, Mechanical design and motion control of a hand exoskeleton for rehabilitation, in: *Mechatronics and Automation*, 2005 IEEE International Conference, Vol. 1, 2005, pp. 155–159. doi:10.1109/ICMA.2005.1626539.
- [15] T. Worsnopp, M. Peshkin, J. Colgate, D. Kamper, An actuated finger exoskeleton for hand rehabilitation following stroke, in: *Rehabilitation Robotics*, 2007. ICORR 2007. IEEE 10th International Conference on, 2007, pp. 896–901. doi:10.1109/ICORR.2007.4428530.
- [16] J. Iqbal, N. Tsagarakis, D. Caldwell, A human hand compatible optimised exoskeleton system, in: *Robotics and Biomimetics (ROBIO)*, 2010 IEEE International Conference on, 2010, pp. 685–690. doi:10.1109/ROBIO.2010.5723409.
- [17] M. Fontana, A. Dettori, F. Salsedo, M. Bergamasco, Mechanical design of a novel hand exoskeleton for accurate force displaying, in: *Robotics and Automation*, 2009. ICRA '09. IEEE International Conference on, 2009, pp. 1704–1709. doi:10.1109/ROBOT.2009.5152591.
- [18] T. Burton, R. Vaidyanathan, S. Burgess, A. Turton, C. Melhuish, Development of a parametric kinematic model of the human hand and a novel robotic exoskeleton, in: *Rehabilitation Robotics (ICORR)*, 2011 IEEE International Conference on, 2011, pp. 1–7. doi:10.1109/ICORR.2011.5975344.
- [19] E. Brokaw, I. Black, R. Holley, P. Lum, Hand spring operated movement enhancer (handsome): A portable, passive hand exoskeleton for stroke rehabilitation, *Neural Systems and Rehabilitation Engineering*, IEEE Transactions on 19 (4) (2011) 391–399. doi:10.1109/TNSRE.2011.2157705.
- [20] P. Polygerinos, Z. Wang, K. C. Galloway, R. J. Wood, C. J. Walsh, Soft robotic glove for combined assistance and at-home rehabilitation, *Robotics and Autonomous Systems* (00) (2014) 00. doi:http://dx.doi.org/10.1016/j.robot.2014.08.014. URL <http://www.sciencedirect.com/science/article/pii/S0921889014001729>
- [21] L. Lucas, M. DiCicco, Y. Matsuoka, An emg-controlled hand exoskeleton for natural pinching, *Journal of Robotics and Mechatronics* 16 (5) (2004) 482 – 488.
- [22] Y. Hasegawa, Y. Mikami, K. Watanabe, Y. Sankai, Five-fingered assistive hand with mechanical compliance of human finger, in: *Robotics and Automation*, 2008. ICRA 2008. IEEE International Conference on, 2008, pp. 718–724. doi:10.1109/ROBOT.2008.4543290.
- [23] A. Chiri, N. Vitiello, F. Giovacchini, S. Roccella, F. Vecchi, M. Carrozza, Mechatronic design and characterization of the index finger module of a hand exoskeleton for post-stroke rehabilitation, *Mechatronics*, IEEE/ASME Transactions on 17 (5) (2012) 884–894. doi:10.1109/TMECH.2011.2144614.
- [24] M. Cempini, S. De Rossi, T. Lenzi, M. Cortese, F. Giovacchini, N. Vitiello, M. Carrozza, Kinematics and design of a portable and wearable exoskeleton for hand rehabilitation, in: *Rehabilitation Robotics (ICORR)*, 2013 IEEE International Conference on, 2013, pp. 1–6. doi:10.1109/ICORR.2013.6650414.
- [25] Festo, Festo exohand characteristics, <http://www.festo.com> (2012).
- [26] H. Kazerooni, Exoskeletons for human power augmentation, in: *Intelligent Robots and Systems*, 2005. (IROS 2005). 2005 IEEE/RSJ International Conference on, 2005, pp. 3459–3464. doi:10.1109/IROS.2005.1545451.
- [27] A. Wege, A. Zimmermann, Electromyography sensor based control for a hand exoskeleton, in: *Proceedings of the 2007 IEEE International Conference on Robotics and Biomimetics*, 2007, pp. 1470–1475.
- [28] Y. Z. Jiting Li, Ruoyin Zheng, J. Yao, ihandrehab: an interactive hand exoskeleton for active and passive rehabilitation, in: *2011 IEEE International Conference on Rehabilitation Robotics*, 2011, pp. 1–6.
- [29] M. Fontana, M. Bergamasco, S. Marcheschi, Haptic hand exoskeleton for precision grasp simulation, *ASME Journal of Mechanisms and Robotics* 5 (4) (2013) 9–18. doi:10.1115/1.4024981.
- [30] A. E. F. Jamshed Iqbal, Nikos G. Tsagarakis, D. G. Caldwell, A portable rehabilitation device for the hand, in: *32nd Annual International Conference of the IEEE EMBS*, 2010, pp. 3694–3697.
- [31] K. Tong, An intention driven hand functions task training robotic system, in: *32nd Annual International Conference of the IEEE EMBS*, 2010, pp. 3406–3409.
- [32] A. Stienen, E. Hekman, F. van der Helm, H. van der Kooij, Self-aligning exoskeleton axes through decoupling of joint rotations and translations, *Robotics*, IEEE Transactions on 25 (3) (2009) 628–633. doi:10.1109/TR0.2009.2019147.
- [33] M. Cempini, S. De Rossi, T. Lenzi, N. Vitiello, M. Carrozza, Self-alignment mechanisms for assistive wearable robots: A kinetostatic compatibility method, *Robotics*, IEEE Transactions on 29 (1) (2013) 236–250. doi:10.1109/TR0.2012.2226381.
- [34] Matlab, Matlab-simmechanics toolbox, <http://www.matlab.com> (2015).
- [35] Kinovea, Kinovea: an open source motion capture software, <http://www.kinovea.org> (2014).
- [36] J. Nocedal, S. J. Wright, *Numerical Optimization*, Second Edition, Springer Series in Operations Research, Springer Verlag, 2006.
- [37] R. Byrd, J. C. Gilbert, J. Nocedal, A trust region method based on interior point techniques for nonlinear programming, *Mathematical Programming* 89 (1) (2000) 149–185.
- [38] K. Watanabe, H. Morishita, T. Mori, T. Sato, A prototype of index-finger pip joint motion amplifier for assisting patients with impaired hand mobility, in: *Robotics and Automation*, 2007 IEEE International Conference on, 2007, pp. 4146–4151. doi:10.1109/ROBOT.2007.364116.
- [39] F. Amirabdollahian, S. Ates, A. Basteris, A. Cesario, J. Burke, H. Hermens, D. Hof, E. Johansson, G. Mountain, N. Nasr, S. Nijenhuis, G. Prange, N. Rahman, P. Sale, B. van Schooten, A. Stienen, Design, development and deployment of a hand/wrist exoskeleton for home-based rehabilitation after stroke - script project, *Robotica* 32 (2014) 1331–1346. doi:10.1017/S0263574714002288.